Hydrodynamics of the Changjiang Estuary and Adjacent Seas

2

Jianrong Zhu, Hui Wu, and Lu Li

Abstract

In this chapter, we use our previous observational and modeling studies to analyze some basic dynamic features of the Changjiang (Yangtze River) Estuary, including the tidal and subtidal motion, saltwater intrusion, and the extension of a river plume into the ocean. The dynamics of this estuary are strongly regulated by tides on both intertidal and subtidal scales. Harmonic analysis shows that the tidal regime has one dominant semidiurnal constituent. The tidal range has significant seasonal variations, but is typically between 4 and 5 m during the spring tide and $\sim$2 m during the neap tide. Tidal forcing induces significant subtidal circulation, resulting in a net landward flow into the North Branch of the Changjiang Estuary when river discharge is low. This residual transport forms a type of saltwater intrusion known as the saltwater-spilling-over (SSO). This causes high-salinity water in the North Branch to intrude upstream and finally spill over into the South Branch, which is the major channel of the estuary. The SSO has a major impact on the Changjiang Estuary and on the availability of freshwater for nearby cities. In areas near the river mouth, the tide-induced residual transport also results in significant inter-channel water mass exchange. Freshwater output from the Changjiang forms a large-scale plume, which plays a key role in physical processes in the adjacent East China Sea and Yellow Sea. We found that, in the region close to the river mouth, tidal forcing has a marked effect on the extension of the plume into the open ocean. Wind forcing also plays an important role in the dynamics of the Changjiang Estuary. Northerly winds can enhance the SSO and saltwater intrusion around the river mouth. In the plume-affected region, the wind significantly modulates the plume shape, especially farther from the river mouth.

Keywords

Tide • Subtidal circulation • Saltwater intrusion • River plume • Wind forcing

J. Zhu (✉) · H. Wu · L. Li
State Key Laboratory of Estuarine and Coastal Research,
East China Normal University, 3663 Zhongshan Road North,
Shanghai 200062, China
e-mail: jrzhu@sklec.ecnu.edu.cn

H. Wu
e-mail: hwu@sklec.ecnu.edu.cn

L. Li
e-mail: lilusklec@gmail.com

J. Zhang (ed.), *Ecological Continuum from the Changjiang (Yangtze River) Watersheds to the East China Sea Continental Margin*, Estuaries of the World,
DOI 10.1007/978-3-319-16339-0_2,

2.1 Introduction

The Changjiang, also known as the Yangtze River in the region between Nanjing and the river mouth, originates in the Tibetan Plateau and flows more than 6000 km through 10 provinces of China, before entering the East China Sea near Shanghai (Fig. 3.1; see Chap. 3). The Changjiang has the fourth largest mean sediment load and fifth largest discharge of rivers worldwide, delivering $\sim 9.24 \times 10^{11}$ m^3/year of freshwater to the Yellow Sea and East China Sea (Shen et al. 2003). The Changjiang is the most important source of terrestrial materials deposited into the East China Sea and the Yellow Sea (see Chaps. 3, 5 and 6).

The Changjiang Estuary has a tidal limit of nearly 640 km, a 90-km-wide river mouth, and is characterized by multiple bifurcations due to sand islands (Fig. 2.1). Downstream from Xuliujing, the estuary is divided by Chongming Island into the South Branch (SB) and North Branch (NB). The SB and its lower reaches form the main channel of the Changjiang and contain most of the river discharge, while the NB is heavily silted. The waterways in the Changjiang Estuary are far wider than most other estuaries, with widths of between ~ 10 and ~ 20 km. The subaqueous delta, adjacent to the Changjiang mouth, occurs at water depths that gradually increase to between 50 and 60 m. The lower SB is bifurcated into the South Channel (SC) and the North Channel (NC) by Changxing Island and Hengsha Island. Finally, the SC is bifurcated into the South Passage (SP) and the North Passage (NP) by Jiuduan **Sandbank**. Thus, four outlets, separated by extensive intertidal flats, discharge from the Changjiang Estuary into the sea.

The natural evolution and artificial reclamation of the intertidal zone from the 1950s to the 1970s have severely narrowed the upper reaches of the NB. As a consequence, the upper reaches have become almost orthogonal to the SB, while the lower reaches have become funnel-shaped (Shen et al. 2003). These modifications not only help to prevent runoff from entering the NB, especially during the dry season, but also make the tidal range larger than in the SB. This high tidal range results in a process known as the saltwater-spilling-over (SSO), whereby saltwater from the NB spills into the SB during dry-season floods.

The Changjiang Estuary is unique among well-studied estuaries, due to its large size, high river discharge, considerable tidal range, and relatively high suspended-sediment concentration (see Chap. 3). It also has an extremely

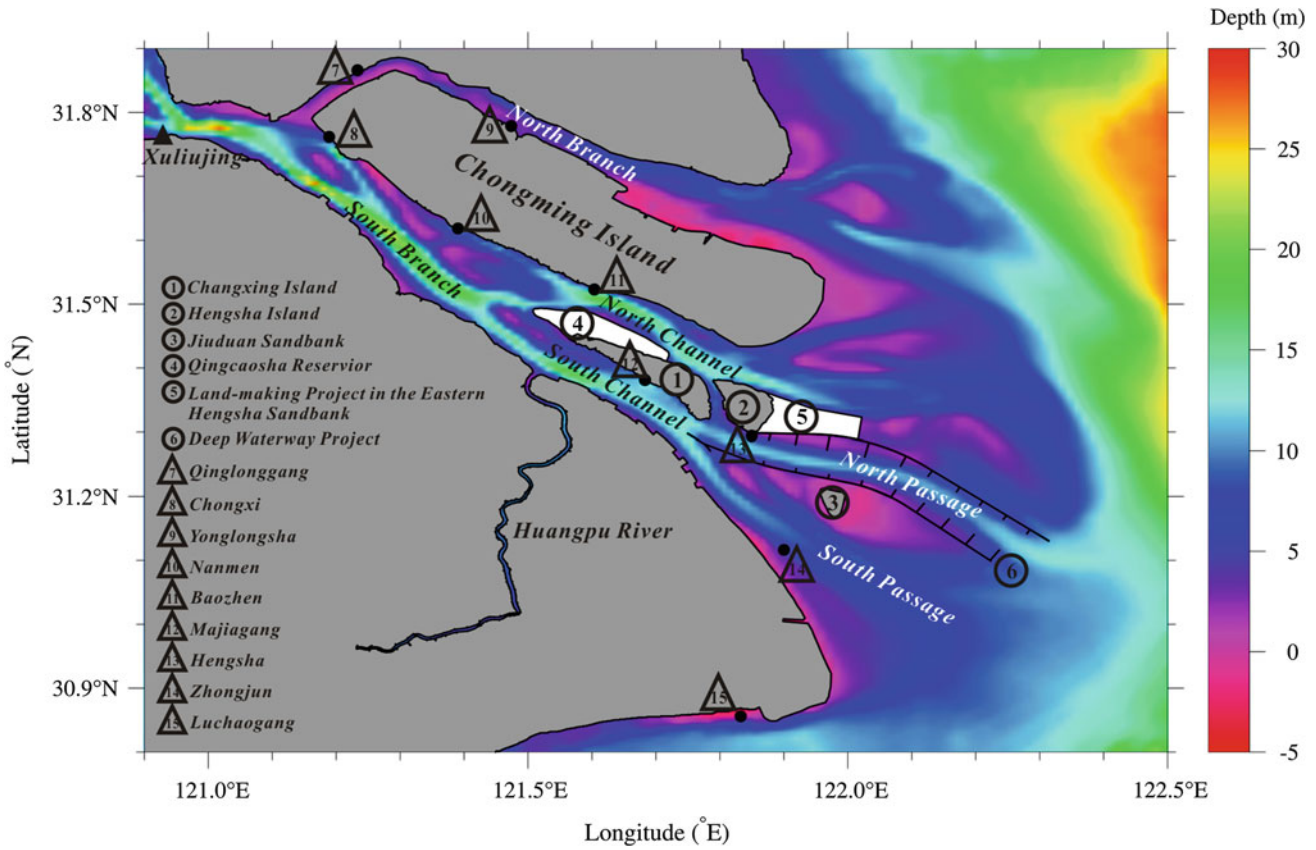

Fig. 2.1 Map of the Changjiang Estuary. Key geographic locations and tide gauges are *numbered* and marked by *circles* and *triangles*, respectively

dynamic hydrological environment due to significant shelf currents off the river mouth and the East Asian monsoon. These dynamics have a strong influence on tides, circulation, saltwater intrusion, plume dispersal, sedimentary erosion/deposition (see Chap. 4), and other biogeochemical processes (see Chaps. 5 and 6).

Runoff, tides, winds, the continental-shelf current, mixing, and topography are the main controls on hydrodynamic processes in the Changjiang Estuary (Wu et al. 2006; Xiang et al. 2009; Li et al. 2012). The river discharge and winds have a strong seasonality. Winds are controlled primarily by the monsoon, which brings weak southerly winds in summer and strong northerly winds in winter. Tides exhibit a medium tidal range and are the most energetic source of water movement in the Changjiang Estuary. The tidal range introduces a significant tidal current, which oscillates and mixes dissolved materials. Saltwater intrusion into the river mouth can also produce estuarine circulation (Pritchard 1956) and change the stratification (Simpson et al. 1990), thereby influencing the movement of sediments and producing maximum estuarine turbidities (Geyer 1993; see Chap. 3).

The East China Sea and the Yellow Sea are adjacent to the Changjiang mouth. The water depths and summertime circulation patterns of these seas are shown in Fig. 2.2. The East China Sea has the flattest and widest continental shelf in the world, which is bounded to the north by a line running northeast from the northern edge of the Changjiang mouth to the southwestern tip of Korea, to the east by the Ryukyu islands chain and Kyushu, to the south by Taiwan, and to the west by the east coast of the Chinese mainland (Fig. 2.2). The Yellow Sea is a shallow, marginal sea bounded to the north by the Bohai Sea, to east by Korea, to south by the East China Sea, and to the west by the east coast of China (Fig. 2.2).

Intense land–ocean interactions occur between the Changjiang Estuary and the adjacent seas. The coastal current brings sediment and other materials into the estuary, and the ocean produces tides and tidal currents that cause

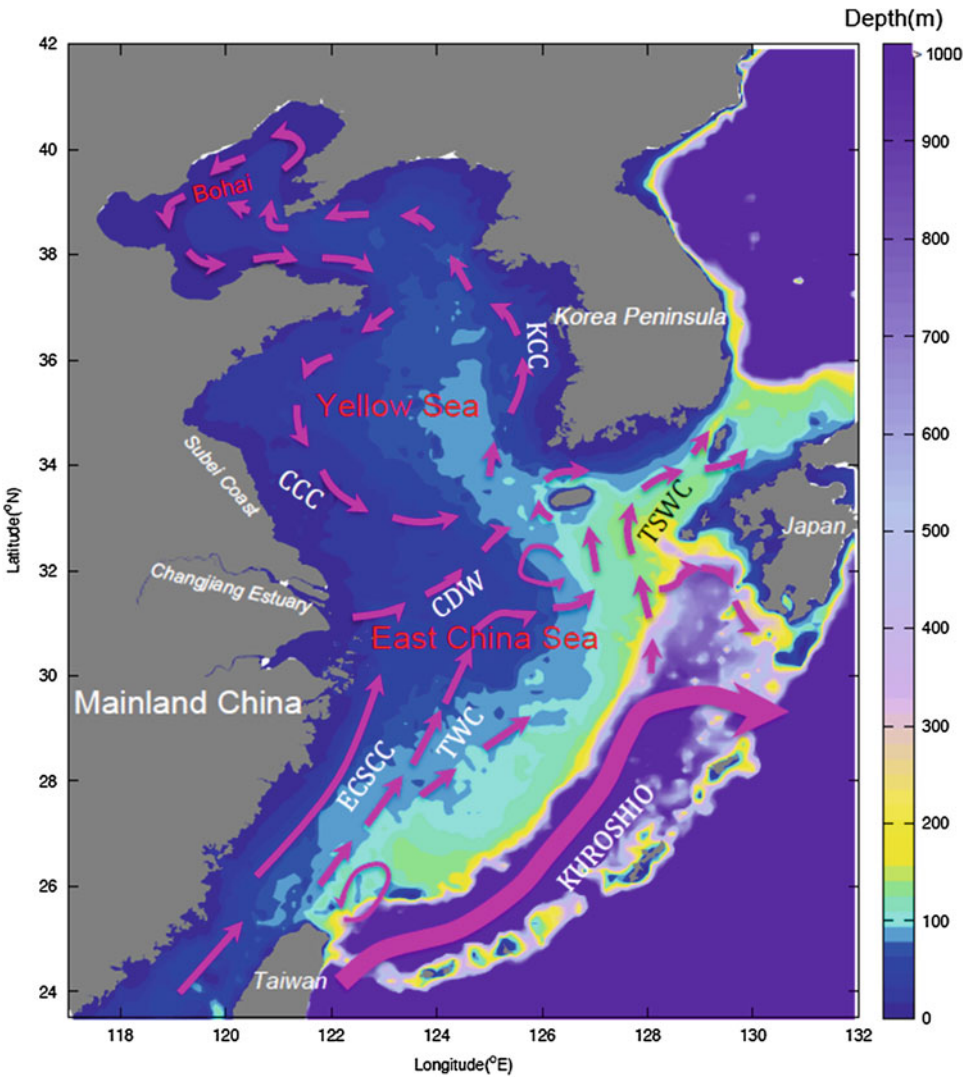

Fig. 2.2 Water depth and summertime circulation patterns in the East China Sea, Yellow Sea, and Bohai Sea. Circulation patterns in the Bohai Sea are adapted from Su and Yuan (2005), and circulation patterns in the East China Sea and Yellow Sea are adapted from Lü et al. (2006). TWC is the Taiwan Warm Current; ECSCC is the East China Sea Coastal Current; CDW is the Changjiang Diluted Water; CCC is the Chinese Coastal Current; KCC is the Korean Coastal Current; and TSWC is the Tsushima Warm Current

saltwater intrusion and that influence circulation, sediment flocculation, the ecological environment, and freshwater availability.

Huge quantities of freshwater from the Changjiang enter the East China Sea and Yellow Sea. This water flux, known as Changjiang diluted water (CDW), is a prominent hydrographic feature in the East China Sea and the Yellow Sea. In summer, it extends northeast and forms a surface plume (Fig. 2.2), and in winter it flows south in a narrow band along the East China coast. The Changjiang carries an enormous volume of water, sediments, and nutrients to the East China Sea and Yellow Sea (see Chaps. 3, 5, and 6), which significantly influences the water properties, circulation structure, sediment deposition, and ecosystems of the adjacent seas (Beardsley et al. 1985; Zhu and Shen 1997).

This chapter describes the hydrodynamics of the Changjiang mouth and the land–ocean interactions in this region. Section 2.2 describes the basic features of the tides and residual water transport, and Sect. 2.3 provides an overview of the impact of wind on saltwater intrusion. Section 2.4 describes the dispersal of the CDW riverine plume across the continental shelf based on observational data and numerical simulations of tidal modulation of plume dispersion.

2.2 Tides and Residual Water Transport

2.2.1 Tides

Tides are the most energetic source of water movement in the Changjiang Estuary (Shen et al. 2003). According to data from Luchaogang hydrographic station (Fig. 2.1) collected in 2006 and 2007, the tidal range exhibits significant monthly, semimonthly, and semidiurnal signals. During the spring tide, the amplitude is generally greater than 450 cm and is approximately twice that of the neap tide, which is typically less than 250 cm. Around the Changjiang Estuary, the tidal amplitude is increased due to shoaling effects. The mean annual tidal range at Zhongjun station, for example, is 267 cm and the maximum tidal range is 462 cm (Shen et al. 2003).

The Changjiang Estuary is influenced by two distinct tidal systems: a progressive tide from the East China Sea and a rotating tide from the Yellow Sea (Choi 1980). The tidal wave from the northwest Pacific propagates nearly parallel to the Ryukyu Islands, entering the East China Sea, and moving northwest toward the Changjiang Estuary. Shallow topography adjacent to the river mouth causes denser cophase lines and a reduction in the velocity of the tidal wave. In the Yellow Sea, the tide rotates with two nodal points (Choi 1980), with the southern node having a dominant influence in the northern Changjiang Estuary. Convergence between the progressive tide and the rotating tide produces a special region along a line from the Subei Coast (Fig. 2.2) to the southwest tip of the Korean Peninsula, where the tide becomes standing.

Because of the complicated river regime, the tide acts in distinct ways in different outlets. For example, as the NB is funnel-shaped, there is significant reflection of the tidal wave, and a standing wave is formed. In the SB, on the other hand, the reflection is relatively weak and the tide propagates evenly, with only minor distortion of the tidal wave.

To conduct a detailed investigation of the tidal characteristics inside the Changjiang mouth, we used tidal data from six hydrological stations: Hengsha, Majiagang, Baozhen, Yonglongsha, Chongxi, and Nanmen (Fig. 2.1). Data were sampled hourly throughout 2009, providing sufficient resolution to reveal the temporal variability of tides in this region.

Although the in situ tidal elevation is a straightforward way to describe water-level fluctuations, as well as the associated fortnightly and seasonal variations, a better method is to decompose the observed data into a series of constituents with different periods using harmonic analysis. Although infinite numbers of harmonic constituents can be generated, it is generally only practical to consider several of the major constituents. In this study, we used harmonic analysis to characterize the key tidal constituents, along with the tidal form and distortion.

2.2.1.1 Tidal Elevation and Tidal Range

The tidal elevation not only exhibited semidiurnal variability, but also had a significant fortnightly variability (Fig. 2.3). Water levels in December were generally lower than in September due to the reduction in river discharge. Mean monthly water levels at the six stations all show significant seasonal variability, reflecting the variability in river discharge, with a peak values around August, and low values in January (Table 2.1). Mean monthly water levels at Yonglongsha station were lower than the other five stations (174 cm in January and 219 cm in August), because the tidal flat at the upper reaches of the NB restrains the runoff into the NB.

Figure 2.3 also clearly illustrates the temporal variation of the tidal range at the six stations in September and December 2009. For example, at Hengsha station, the maximum tidal range of 360 cm occurred during a spring tide on September 20 and was only 130 cm on September 27 during a neap tide. The difference between the spring and neap tidal ranges was primarily due to differences in the high-tide water level, which was more variable during the neap tide. Two high-tide water levels on September 14 during a neap tide were 235 and 305 cm, with a difference exceeding half of the tidal range at that time.

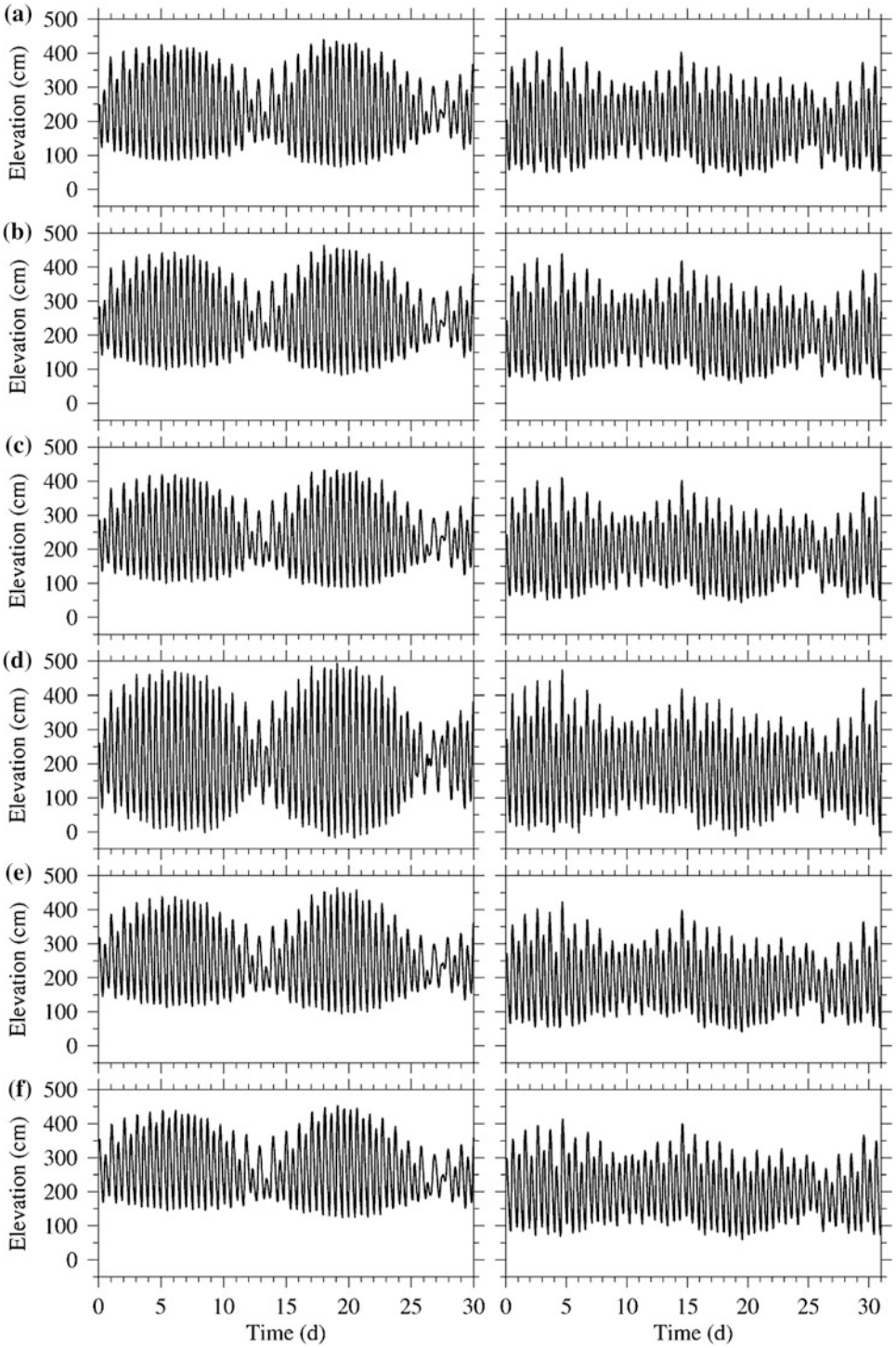

Fig. 2.3 Temporal variation of the measured water level (tidal elevation) in 2009 at: **a** Hengsha station; **b** Majiagang station; **c** Baozhen station; and **d** Yonglongsha station, during September (*left panels*) and December (*right panels*)

Such diurnal inequality is mainly caused by the gravitational pull of the earth, moon, and sun. The maximum tidal range in December was also smaller than in September when the earth, moon, and sun are aligned and the gravitational pull combines to produce a spring tide. The fortnightly variability of the tidal range was weaker in December than in September. The seasonal and fortnightly variations in September and December at the other five stations are comparable to those at Hengsha station (Fig. 2.3b–d). Of note, the tidal range at Yonglongsha station exceeded 500 cm and reached 400 cm in December. This range is considerably larger than at other stations due to the location of Yonglongsha station in the NB, where the funnel-shaped topography concentrates flow and the tidal forcing is stronger than river discharge.

Table 2.1 Mean monthly water level (cm) at each hydrological station

Month	1	2	3	4	5	6	7	8	9	10	11	12
Hengsha	178	189	191	196	206	215	217	236	234	215	206	195
Majiagang	184	198	204	207	217	225	230	251	249	228	220	210
Baozhen	178	190	196	198	208	220	226	243	238	213	205	192
Yonglongsha	174	185	182	185	191	201	202	219	216	201	201	188
Chongxi	191	205	218	221	236	250	256	277	267	234	219	206
Nanmen	181	195	203	204	215	234	237	257	250	221	206	193

To further investigate the variability in tidal intensity, statistical analyses of the tidal range at these six stations were conducted (Table 2.2). These results indicate that the tidal range is highly seasonal, generally reaching its maximum in March and September, and its minimum in June and December. For example, at Hengsha station, the maximum spring tide range occurred in March and September with values of 352 and 364 cm, respectively, and the minimum spring tide range occurred in May and December with values of 309 and 298 cm, respectively. The neap tide range also had two peaks, but these were anti-phased with the spring tide range. The maximum neap tide ranges occurred during June and December with values of 167 and 137 cm, respectively, and the minimum neap tide ranges occurred in February and September with values of 78 and 87 cm, respectively.

Overall, the tidal range annual variability was the same at the six gauging stations. In the SB, the tidal range progressively decreased upstream. The tidal range at Baozhen station was the largest, followed by Hengsha station, and then Nanmen and Chongxi stations, which are inside the SB. This pattern is caused by energy dispersion due to friction when the tidal wave propagates up the estuary. Moreover, the effects of river discharge become stronger upstream, which also reduces the tidal range. Yonglongsha station is located in the NB and, although the seasonal variation was similar to at the other stations, the tidal range was larger. The tidal range of the NB is amplified due to the comparatively low river discharge in this channel, as well as the funnel-shaped topography, which concentrates the tidal energy.

2.2.1.2 Harmonic Analysis

To further investigate the tidal form in the Changjiang Estuary, we used the harmonic analysis program T_TIDE to identify the tidal constituents from the tidal elevation data. The tide in the Changjiang Estuary is regulated by four semidiurnal constituents (M_2, S_2, N_2, and K_2); four diurnal constituents (K_1, O_1, P_1, and Q_1); and three shallow-water constituents (M_4, MS_4, and M_6). Table 2.3 gives the amplitude and phase of each constituent at all gauging stations. The semidiurnal constituents were dominant overall, and the largest constituents within this group were M_2 and S_2. Furthermore, M_2 has an amplitude that is approximately twice that of S_2.

At Hengsha station, the amplitude of M_2 was 114 cm and the amplitude of the other semidiurnal constituents S_2, N_2, and K_2 were 49, 19, and 14 cm, respectively. The diurnal constituents had considerably smaller amplitudes. Of this

Table 2.2 Maximum and minimum monthly tidal range (cm) at each hydrological station

Month	Hengsha		Majiagang		Baozhen		Yonglongsha		Chongxi		Nanmen	
	Spring	Neap	Spring	Neap	Spring	Neap	Spring	Neap	Spring	Neap	Spring	Neap
1	311	122	305	121	294	106	410	135	272	112	300	112
2	332	78	330	77	317	66	442	107	295	68	320	105
3	352	80	336	75	321	64	455	50	292	67	327	68
4	319	86	320	83	303	74	431	112	281	75	313	74
5	309	137	312	130	293	117	433	184	277	114	302	120
6	317	167	322	156	306	144	443	221	283	137	310	144
7	350	122	349	114	324	102	475	140	301	97	333	101
8	356	97	358	92	333	85	517	64	309	82	344	84
9	364	87	368	83	338	79	500	62	322	81	360	82
10	339	89	350	90	331	81	459	125	312	86	340	83
11	311	125	318	123	306	115	419	156	285	117	314	118
12	298	136	303	128	293	118	382	165	275	117	298	121

Table 2.3 Tidal harmonic constants (amplitude and phase) of the major tidal constituents at each tide gauge

Constituents	Hengsha		Majiagang		Baozhen		Yonglongsha		Chongxi		Nanmen	
	amp	phs	amp	phs	amp	phs	amp	phs	amp	phs	amp	phs
M_2	114	112	109	128	101	1401	137	143	93	185	100	161
S_2	49	153	47	168	44	179	61	182	39	226	43	201
N_2	19	102	19	117	18	130	25	133	16	172	18	149
K_2	14	147	13	164	13	173	18	174	11	222	12	196
K_1	25	83	25	90	23	90	23	71	22	115	23	102
O_1	16	43	16	49	15	48	13	30	15	72	15	60
P_1	6	93	6	98	6	99	6	93	6	121	6	110
Q_1	3	30	3	34	2	34	2	21	2	54	2	44
M_4	16	151	16	187	16	209	24	219	19	286	20	245
MS_4	13	192	14	229	14	251	22	265	16	328	17	288
M_6	4	149	4	184	2	238	3	213	4	149	4	301

group, K_1 was the strongest with an amplitude of 25 cm, followed by O_1 with an amplitude of 16 cm. Notably, the shallow-water tidal constituents around the Changjiang Estuary were relatively high, and the amplitudes of M_4 and MS_4 were both around 15 cm. M_6 was a very minor constituent with an amplitude of less than 5 cm. The phases of the semidiurnal tides were between 102° and 153°, and the phases of the diurnal tides were between 43° and 93°. The phases of shallow-water tides were larger overall; e.g., MS_4 had a phase of 192°.

The amplitudes and phases of each tidal constituent at Majiagang and Baozhen stations were similar to those at Hengsha station. Semidiurnal tides were dominant, but shallow-water constituents were also significant. The semidiurnal and diurnal tides at Nanmen and Chongxi stations were slightly smaller, and the shallow-water constituents were larger compared with downstream stations. However, due to bottom friction, their amplitudes were suppressed, particularly for the semidiurnal tidal constituents. Moreover, tidal distortion became more severe farther up the estuary, which is particularly evident in the increased amplitudes and phase of the M_4 and MS_4 constituents.

The tidal phase at Yonglongsha station was similar to the other stations. Amplitudes of the semidiurnal tidal constituents at Yonglongsha station were larger than at other stations, particularly for M_2, which had an amplitude of 137 cm. However, the amplitudes of the diurnal tides were comparatively small at this station, with an amplitude of only 22 cm for K_1. This indicates that the tidal form is more semidiurnal in the NB than in the SB. Moreover, the shallow-water tides at Yonglongsha station were amplified, with the amplitudes for M_4 and MS_4 being 50 % greater than those at Hengsha station. This indicates that the tidal distortion in the NB is also more pronounced. In extreme tides, a tidal bore occurs in the NB.

Based on the results of the harmonic analysis, the tidal form can be classified using the ratio of semidiurnal to diurnal tidal amplitudes:

$$F = (H_{O1} + H_{K1})/(H_{M2} + H_{S2}) \tag{2.1}$$

where F is the tidal form number, and H_{o1}, H_{k1}, H_{m2}, and H_{s2} are the amplitudes of the tidal constituents of O_1, K_1, M_2, and S_2, respectively.

Tidal form is classified as regular semidiurnal when $0.0 < F \leq 0.25$; irregular semidiurnal when $0.25 < F \leq 1.5$; irregular diurnal when $1.5 < F \leq 3.0$; and regular diurnal when $F > 3.0$ (Chen 1980). F was greater than 0.25 at all stations aside from Yonglongsha station, where it was less than 0.25 (Table 2.4), indicating that the tidal form is regular semidiurnal in the NB and irregular semidiurnal in the SB, NC, SC, and NP.

Because of the influences of the friction, runoff, and topography, the tidal wave is often distorted in the shallow estuary region. The distortion can be quantified using the ratio of M_4 to M_2 amplitudes; i.e., $A = H_{M4}/H_{M2}$. The flood/ebb asymmetry can be quantified using phase difference; i.e., $G = 2\varphi_{M2} - \varphi_{M4}$. When $0° < G \leq 180°$, the ebb duration is longer than the flood duration, and the flood current is stronger than the ebb current. In contrast, when $180° < G \leq 360°$, the flood duration is longer than the ebb duration, and the ebb current is stronger than the flood current.

The value of A was greater than 0.1 at all stations (Table 2.4), indicating that tide distortion due to shallow water is significant in the Changjiang Estuary. The tide distortion was comparatively small at Hengsha station ($A = 0.137$), but stronger at Yonglongsha station ($A = 0.173$). The G values at all six stations were between 68.10 and 84.84, indicating that the ebb duration was longer than the

Table 2.4 The tidal form number, F, and the tidal distortion coefficients, A and G, at each tide gauge

	Hengsha	Majiagang	Baozhen	Yonglongsha	Chongxi	Nanmen
F	0.252	0.259	0.258	0.178	0.283	0.268
A	0.137	0.150	0.159	0.173	0.206	0.204
G	73.66	68.10	72.9	68.17	84.84	77.13

flood duration, and the flood current was stronger than the ebb current.

Although G values reveal the asymmetry of the ebb/flood duration in the Changjiang Estuary, they fail to represent spatial variability of ebb/flood currents. In the SB, SC, and NC, for example, the ebb current is stronger, while in the NB the flood current is stronger. Due to the very high river discharge, the ebb current is generally more dominant in the Changjiang Estuary (Qiu and Zhu 2013), which is in contrast to the results produced using G values. Because G considers only the tidal constituents and neglects the effects of river discharge, it should be used with caution in the areas with very high river discharge, such as the Changjiang Estuary.

2.2.2 Residual Water Transport

Subtidal circulation, also known as residual water transport, governs the long-term transport of salt and other soluble and conservation materials. Subtidal circulation in estuaries is mainly induced by low-frequency forces, such as runoff and wind, baroclinic gradient forces, and the tide itself (Pritchard 1956).

The most commonly used method to calculate residual movement is the Euler residual current, which uses arithmetic averages or low-pass filters to cut off the periodically oscillating component of the tidal current. However, in regions where the tidal range is large relative to the water depth, the Euler residual current might be misleading. To solve this problem, Ianniello (1977) introduced the nonlinear factor $\varepsilon = \zeta/D$, where ζ is the tidal range and D is the total depth. The Euler residual is reasonable only if ε is <0.3. In the extensive shallow intertidal zone of the Changjiang Estuary, ε is undoubtedly >0.3, so the Euler residual current is not a suitable method for describing mass transport in this region. Another method that can be used to calculate the residual is the Lagrangian residual, but this method requires a tracer study, is strongly related to the phase at which the tracking particle is released, and is computationally expensive.

We used the residual water transport method to describe the net water mass flux. The water mass flux is defined as the amount of water mass that passes through an area in a unit of time. In this method, the unit width flux is averaged over one or several tidal cycles to calculate the residual (net) unit width water mass flux (NUWF). The NUWF represents the tidally averaged transport rate and direction of water mass at a specified location and is calculated as follows:

$$\overrightarrow{R}(x,y) = \frac{1}{T}\int_0^T \int_{-H(x,y)}^{\zeta} \overrightarrow{V}(x,y,z,t)\mathrm{d}z\mathrm{d}t \tag{2.2}$$

where $\overrightarrow{R}(x,y)$ is the NUWF, T is one or several tidal cycles, $H(x,y)$ is the steady depth water, ζ is the surface elevation, and $\overrightarrow{V}(x,y,z,t)$ is the horizontal current vector.

2.2.2.1 Numerical Model

ECOM-si was developed based on the POM (Princeton Ocean Model) (Blumberg and Mellor 1987; Blumberg 1994) with several improvements (Chen et al. 2001) to address the demand for numerical simulations of water bounded by complicated coastlines. This model incorporates the Mellor and Yamada level 2.5 turbulent closure scheme to provide a time-and-space-dependent parameterization of vertical turbulent mixing (Mellor and Yamada 1974, 1982; Galperin et al. 1988).

Under the assumption of incompressibility, using the Boussinesq and hydrostatic approximations, and introducing the horizontal non-orthogonal curvilinear and vertical-stretched sigma coordinate system, the governing equations of ocean circulation and water mass (consisting of momentum, continuity, temperature, salinity, and density equations) are as follows:

$$\begin{aligned}
&\frac{\partial DJu_1}{\partial t} + \frac{\partial DJ\hat{U}u_1}{\partial \xi} + \frac{\partial DJ\hat{V}u_1}{\partial \eta} + \frac{\partial J\omega u_1}{\partial \sigma} \\
&\quad - Dh_2\hat{V}\left[v_1\frac{\partial}{\partial \xi}\left(\frac{J}{h_1}\right) - u_1\frac{\partial}{\partial \eta}\left(\frac{J}{h_2}\right) + Jf\right] \\
&\quad - Dh_2u_1v_1\frac{\partial}{\partial \xi}\left(\frac{h_3}{h_1h_2}\right) \\
&\quad = -h_2gD\frac{\partial \zeta}{\partial \xi} + \frac{gh_2D}{\rho_o}\frac{\partial D}{\partial \xi}\int_{\sigma}^{0}\sigma\frac{\partial \rho}{\partial \sigma}\mathrm{d}\sigma \\
&\qquad - \frac{gh_2D^2}{\rho_o}\frac{\partial}{\partial \xi}\int_{\sigma}^{0}\rho\mathrm{d}\sigma + \frac{1}{D}\frac{\partial}{\partial \sigma}\left(K_m\frac{\partial Ju_1}{\partial \sigma}\right) + DJF_x,
\end{aligned} \tag{2.3}$$

$$\frac{\partial DJv_1}{\partial t}+\frac{\partial DJ\hat{U}v_1}{\partial \xi}+\frac{\partial DJ\hat{V}v_1}{\partial \eta}+\frac{\partial J\omega v_1}{\partial \sigma}+Dh_1\hat{U}\left[v_1\frac{\partial}{\partial \xi}\left(\frac{J}{h_1}\right)-u_1\frac{\partial}{\partial \eta}\left(\frac{J}{h_2}\right)+Jf\right]-Dh_1u_1v_1\frac{\partial}{\partial \eta}\left(\frac{h_3}{h_1h_2}\right)=-h_1gD\frac{\partial \zeta}{\partial \eta}+\frac{gh_1D}{\rho_o}\frac{\partial D}{\partial \eta}\int_\sigma^0\sigma\frac{\partial \rho}{\partial \sigma}\mathrm{d}\sigma-\frac{gh_1D^2}{\rho_o}\frac{\partial}{\partial \eta}\int_\sigma^0\rho\mathrm{d}\sigma+\frac{1}{D}\frac{\partial}{\partial \sigma}\left(K_m\frac{\partial Jv_1}{\partial \sigma}\right)+DJF_y, \quad (2.4)$$

$$\frac{\partial \zeta}{\partial t}+\frac{1}{J}\left[\frac{\partial}{\partial \xi}\left(DJ\hat{U}\right)+\frac{\partial}{\partial \eta}\left(DJ\hat{V}\right)\right]+\frac{\partial \omega}{\partial \sigma}=0 \quad (2.5)$$

$$\frac{\partial JD\theta}{\partial t}+\frac{\partial JD\hat{U}\theta}{\partial \xi}+\frac{\partial JD\hat{V}\theta}{\partial \eta}+\frac{\partial J\omega\theta}{\partial \sigma}=\frac{1}{D}\frac{\partial}{\partial \sigma}\left(K_h\frac{\partial J\theta}{\partial \sigma}\right)+DJF_\theta \quad (2.6)$$

$$\frac{\partial JDs}{\partial t}+\frac{\partial JD\hat{U}s}{\partial \xi}+\frac{\partial JD\hat{V}s}{\partial \eta}+\frac{\partial J\omega s}{\partial \sigma}=\frac{1}{D}\frac{\partial}{\partial \sigma}\left(K_h\frac{\partial Js}{\partial \sigma}\right)+DJF_s \quad (2.7)$$

$$\rho_{\text{total}}=\rho_{\text{total}}(\theta,s) \quad (2.8)$$

where,

$$\omega=w-\sigma\left(\hat{U}\frac{\partial D}{\partial \xi}+\hat{V}\frac{\partial D}{\partial \eta}\right)-\left[(1+\sigma)\frac{\partial \zeta}{\partial t}+\hat{U}\frac{\partial \zeta}{\partial \xi}+\hat{V}\frac{\partial \zeta}{\partial \eta}\right] \quad (2.9)$$

In the above equations, the new coordinate (ξ, η, σ) is defined as: $\xi=\xi(x,y),\quad \eta=\eta(x,y),\quad \sigma=\frac{z-\zeta}{H+\zeta}$

The vertical coordinate σ varies from −1 at $z=-H$ to 0 at $z=\zeta$, where x, y, and z are the east, north, and vertical axes of the Cartesian coordinate, respectively; ζ is the sea surface elevation; and H the total water depth. The ξ and η components of velocity (defined as u_1, v_1) can be expressed in the form $u_1=\frac{h_2}{J}(x_\xi u+y_\xi v),\quad v_1=\frac{h_1}{J}(x_\eta u+y_\eta v)$, in which the u, v and x, y velocity components are $\xi_x=\frac{y_\eta}{J},\quad \xi_y=-\frac{x_\eta}{J}$, $\eta_x=-\frac{y_\xi}{J},\quad \eta_y=\frac{x_\xi}{J}$, where J is the Jacobin function in the form of $J=x_\xi y_\eta-x_\eta y_\xi$, and the subscript symbols (ξ and η) indicate derivatives. The metric factors h_1 and h_2 of the coordinate transformation are defined as $h_1=\sqrt{x_\xi^2+y_\xi^2}$, $h_2=\sqrt{x_\eta^2+y_\eta^2}$, $\hat{U}=\frac{1}{J}\left(h_2u_1-\frac{h_3}{h_1}v_1\right),\quad \hat{V}=\frac{1}{J}\left(h_1v_1-\frac{h_3}{h_2}u_1\right)$, in which $h_3=y_\xi y_\eta+x_\xi x_\eta$, where θ is the water temperature, s is the salinity, f is the Coriolis parameter, g is the gravitational acceleration, K_m is the vertical eddy viscosity coefficient, and K_h is the thermal vertical eddy friction coefficient. F_u, F_v, F_θ and F_s represent the horizontal momentum, thermal, and salt diffusion terms, respectively. ρ and ρ_o are the perturbation and reference density, which satisfy $\rho_{\text{total}}=\rho+\rho_o$. F_u, F_v, F_θ and F_s are calculated by Smagorinsky's (1963) formula in which horizontal diffusion is directly proportional to the product of horizontal grid sizes. K_m and K_h are calculated using the modified Mellor and Yamada (1974, 1982) level 2.5 turbulent closure scheme.

The surface and bottom boundary conditions for the momentum and heat equations are given by:

$$\begin{aligned}\frac{\rho_0K_m}{D}\left(\frac{\partial u_1}{\partial \sigma},\frac{\partial v_1}{\partial \sigma}\right)&=(\tau_{0\xi},\tau_{0\eta});\ \frac{\rho_0K_H}{D}\left(\frac{\partial \theta}{\partial \sigma}\right)\\&=Q_{\text{net}};\ \frac{\rho_0K_H}{D}\left(\frac{\partial s}{\partial \sigma}\right)\\&=s(\hat{P}-\hat{E});\ \omega=0,\ \text{at}\ \sigma=0,\\\frac{\rho_0K_m}{D}\left(\frac{\partial u_1}{\partial \theta},\frac{\partial v_1}{\partial \theta}\right)&=(\tau_{b\xi},\tau_{b\eta});\ \frac{\partial \theta}{\partial \sigma}\\&=0;\frac{\partial s}{\partial \sigma}=0;\ \omega=0,\ \text{at}\ \sigma=-1\end{aligned}$$

where $(\tau_{o\xi}, \tau_{o\eta})$ and $(\tau_{b\xi},\tau_{b\eta})=C_d\sqrt{U^2+V^2}(U^2+V^2)$ are the ξ and η components of surface wind and bottom stresses; Q_{net} is the net surface heat flux; $\hat{P}$ is the precipitation flux; and $\hat{E}$ is the evaporation flux. The surface wind stress was calculated based on the neutral steady-state drag coefficient developed by Large and Pond (1981). The drag coefficient C_{d} at the bottom is determined by matching a logarithmic bottom layer to the model at a height z_{ab} above the bottom; i.e.,

$$C_{\text{d}}=\max\left[k^2/\ln\left(\frac{z_{\text{ab}}}{z_0}\right)^2,0.0025\right]$$

where k = 0.4 is Karman's constant, and z_0 is the bottom roughness parameter.

Equations 2.3–2.9 are solved prognostically as initial value-problems of oceanic motion. The initial velocity takes the form $u_1=v_1=0$, and the water elevation is also set to be ζ = 0. The initial temperature and salinity are specified using observational data.

This model was developed by Wu and Zhu (2010) with the third HSIMT-TVD scheme to solve the advection term in the mass transport equation. This scheme is flux-based with third-order accuracy in space, second-order accuracy in time, and no numerical oscillation. A wet/dry scheme was included to characterize the intertidal zone due to tidal excursion, and the critical depth was set to 0.2 m.

The model domain covered the whole Changjiang Estuary, Hangzhou Bay, and adjacent seas from 117.5 to 125 °E in

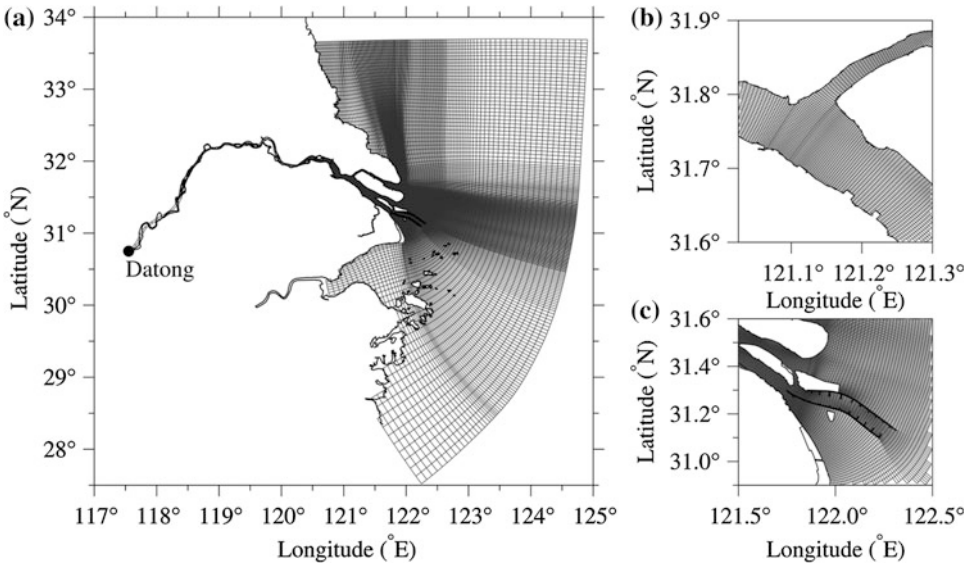

Fig. 2.4 **a** The numerical model mesh; **b** an enlarged view of the model mesh around the bifurcation of the NB and the SB; and **c** an *enlarged view* of the model mesh in the NP, showing the location of the Deep Waterway Project

longitude and 27.5 to 33.7 °N in latitude (Fig. 2.4a). The model grid mesh was composed of 307 × 224 cells horizontally and 10 uniform σ levels vertically. The mesh was designed to fit the coastline, with high-resolution grids near the Changjiang mouth, especially near the bifurcation of the SB and NB (Fig. 2.4b), and the NP where a deep waterway is maintained for navigation (Fig. 2.4c). A lower-resolution grid was used in open water. The grid resolution ranged from 300 to 600 m in proximity to the river mouth and was 15 km near open water. To simulate the SSO in our study, we reduced the grid near the upper NB to a resolution of about 100 m.

According to the *NaoTide* dataset (http://www.miz.nao.ac.jp/), the open sea boundary is driven by 16 astronomical constituents: M_2, S_2, N_2, K_2, K_1, O_1, P_1, Q_1, MU_2, NU_2, T_2, L_2, $2N_2$, J_1, M_1, and OO_1. The river boundary in the model is the location of Datong hydrographic station, which is 630 km upstream from the river mouth. Over the period 1950–2010, water levels are driven by daily river discharge on meteorological time scales and by mean monthly values on climatological time scales.

Wind fields, used to calculate sea surface momentum, were obtained from either the National Center for Environmental Prediction (NCEP) reanalysis dataset with a spatial resolution of 0.5° × 0.5° and a temporal resolution of 6 h, or from hydrological stations in the Changjiang Estuary. Figure 2.5 shows the semimonthly mean wind vectors in the Changjiang Estuary and illustrates that northerly wind prevails from September to March; southerly wind prevails from April to August; and wind speed is much stronger in winter than in summer.

The initial salinity and temperature are from data collected inside the river mouth and from the Ocean Atlas (Editorial Board for marine Atlas 1992). The velocity and elevation were initially set to zero. A detailed description of the model configuration and validation can be found in Wu et al. (2010, 2011) and Li et al. (2012).

2.2.2.2 Residual Water Transport in Winter

The NUWF for spring and neap tides was calculated using the numerical model for a winter case study. In this case, the mean monthly river discharge was 11 × 10^3 m^3/s, the mean northerly wind is 5 m/s, and a baroclinic force is induced by the salinity gradient in January.

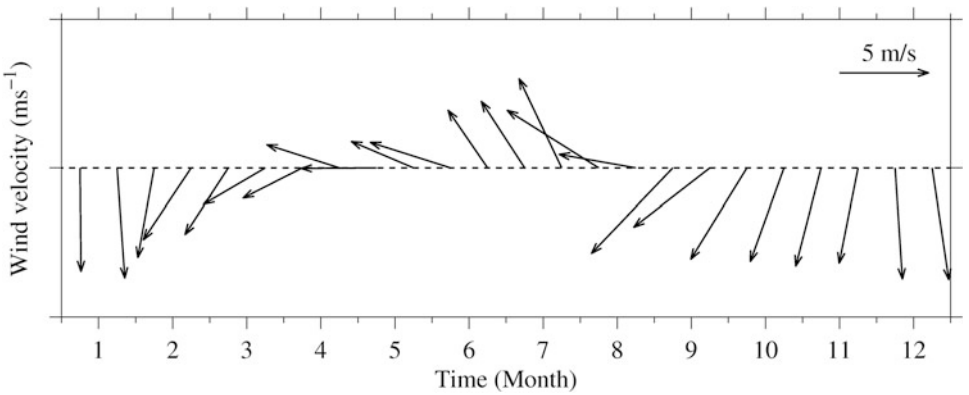

Fig. 2.5 Mean semimonthly wind vectors in the Changjiang Estuary

Figure 2.6a shows the winter NUWF during spring tides. In the SB, SC, NC, and NP, river discharge causes the NUWF to move seaward, and it has a higher magnitude in these channels than in the tidal flats (Fig. 2.6a). In the SP, the NUWF is landward because of the funnel shape produced by the south dyke and the strong salinity front. In sand bar areas, water is transported north across the tidal flats, which is consistent with observational results (Wu et al. 2010). The NUWF in the tidal flat east of Chongming Island is northward due to the tide-induced Stokes drift. In the NB, the NUWF is weaker and landward, and there is net water transport toward the SB.

Figure 2.6b shows the winter NUWF during neap tides. This has similar characteristics to spring tides (Fig. 2.6a) in the SB, SC, NC, and NP, but the magnitude is smaller. Because the tide is weaker, there is net seaward water transport in the southern tidal flats of the SP, and there is no northward water transport across the tidal flats at the river mouth. The effect of the northerly wind stress becomes obvious during neap tides, as the NUWF adjacent to the river mouth flows south. In the NB, the NUWF is even weaker, and there is no net water transport into the SB from the NB.

2.2.2.3 Residual Water Transport in Summer

The NUWF for spring and neap tides was calculated using the numerical model for a summer case study. In this case, the mean monthly river discharge was 49×10^3 m^3/s, the mean southerly wind was 4 m/s, and a baroclinic force was induced by the salinity gradient in July.

Figure 2.7a shows the summer NUWF during spring tides. In the SB, SC, NC, and NP, the NUWF is seaward and has a greater magnitude than for neap tides due to the high river discharge. In the SP, the NUWF is landward and has a lower magnitude than in other channels. The NUWF in the tidal flat east of Chongming Island is northward due to tidal pumping and southerly winds. In the NB, the NUWF is weaker and almost seaward, and the net water transport is into the NB from the SB.

Figure 2.7b shows the summer NUWF during neap tides. In the SB, SC, NC, SP, and NP, the pattern and magnitude of the NUWF are similar to spring tides (Fig. 2.7a), and most of the river water flows into the East China Sea and Yellow Sea through the SB, SC, SP, and NP.

2.3 Saltwater Intrusion

Saltwater intrusion into the Changjiang Estuary is controlled mainly by river discharge, which has a distinct seasonal variability, and by the tidal range (Shen et al. 2003; Wu et al. 2006; Li et al. 2010; Zhu et al. 2010), but is also influenced by wind stress and shelf circulation (Xiang et al. 2009; Wu et al. 2010; Li et al. 2012). Yang et al. (see Chap. 4) report that increased water consumption and dam construction have reduced the annual water discharge by 10 % in the last 150 years. This decrease is primarily attributable to the sharp reduction between August and November when the reservoirs primarily store water. In contrast, the water discharge in the dry season (January and February) has been increasing significantly due to water release from reservoirs (Qiu and Zhu 2013), and the decrease in river discharge in these months intensifies saltwater intrusion into the estuary.

The tide also controls saltwater intrusion into the estuary. On intertidal timescales, the semidiurnal tide drives saltwater into the estuary during flood tides and out of the estuary during ebb tides. The fortnightly spring tide generates greater saltwater intrusion than during the neap tide. Saltwater intrusion is also enhanced by the seasonal variability of tides. The tidal range reaches its maximum during March, and northerly winds produce landward Ekman water transport, which intensifies saltwater intrusion into the NB and the NC (Wu et al. 2010; Li et al. 2012). The Taiwan Warm Current (hereafter referred to as the TWC) and the Chinese Coastal Current (hereafter referred to as the CCC) (Fig. 2.2) also carry high-salinity water into the estuary (Xiang et al. 2009).

Because the Changjiang Estuary is bifurcated, the pattern of saltwater intrusion is different in the NB and SB. In the dry season, when river discharge is low, the NB almost always contains high-salinity water when tides are strong (Shen et al. 2003; Wu et al. 2006). In the lower reaches of the SB, saltwater mainly intrudes landward in a wedge-like manner, as is seen in other partially mixed estuaries (Shen et al. 2003).

The most remarkable feature of saltwater intrusion in the Changjiang Estuary is the SSO from the NB into the SB in the dry season (Box. 2.1). During the spring tide, the water level rises considerably in the upper reaches of the NB due to its funnel shape, leading to a massive amount of saltwater-spilling-over the shoals into the SB. Only a small amount of the saltwater returns to the NB because the shoals are exposed to the air during the ebb tide. The saltwater that is spilled into the SB is transported downstream along with the river discharge and arrives in the middle reaches of the SB during the subsequent neap tide. This effect impacts the Chenhang and Qingcaosha reservoirs and threatens Shanghai's water supply (Box 2.1).

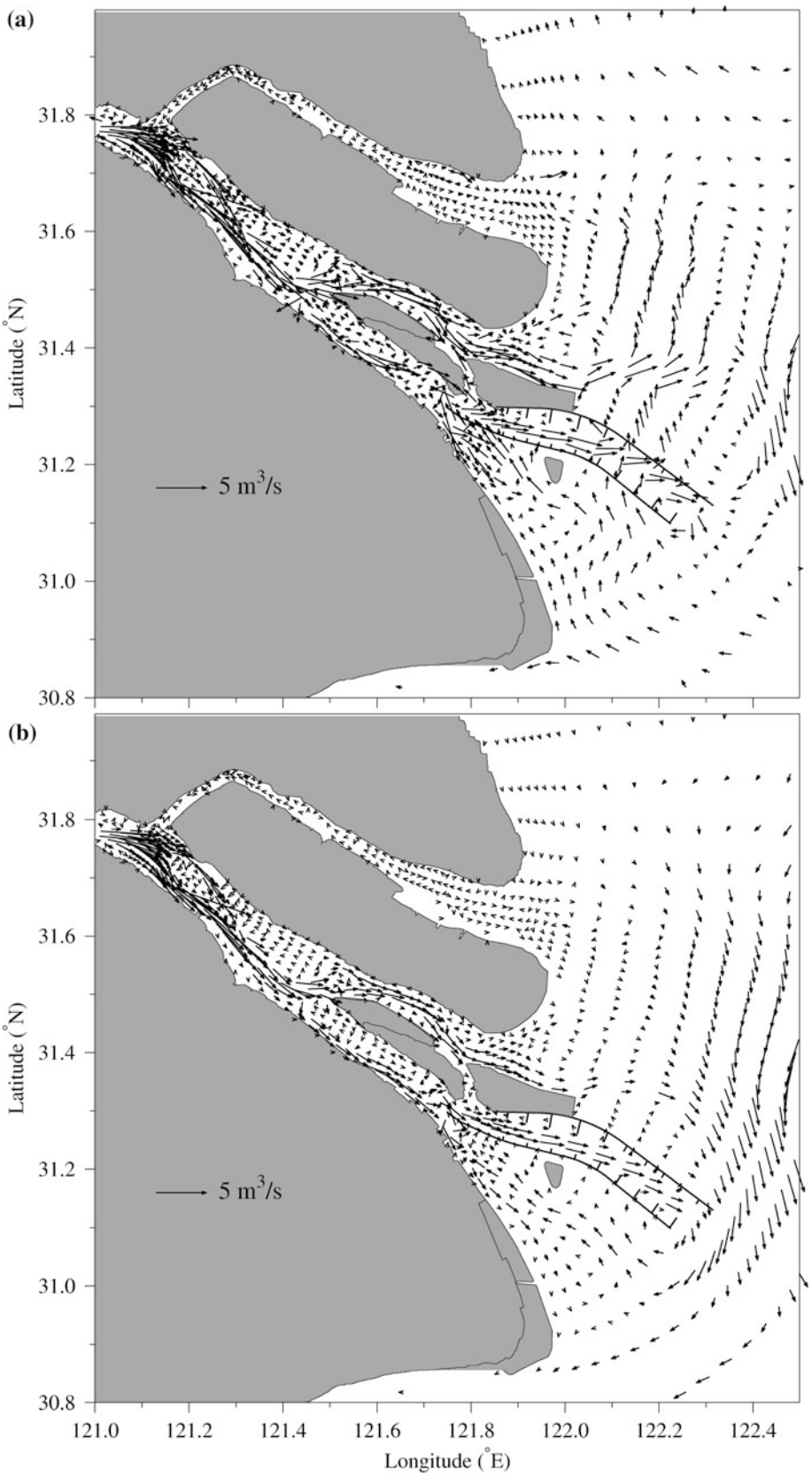

Fig. 2.6 Distribution of the NUWF during winter for: **a** spring tides; and **b** neap tides

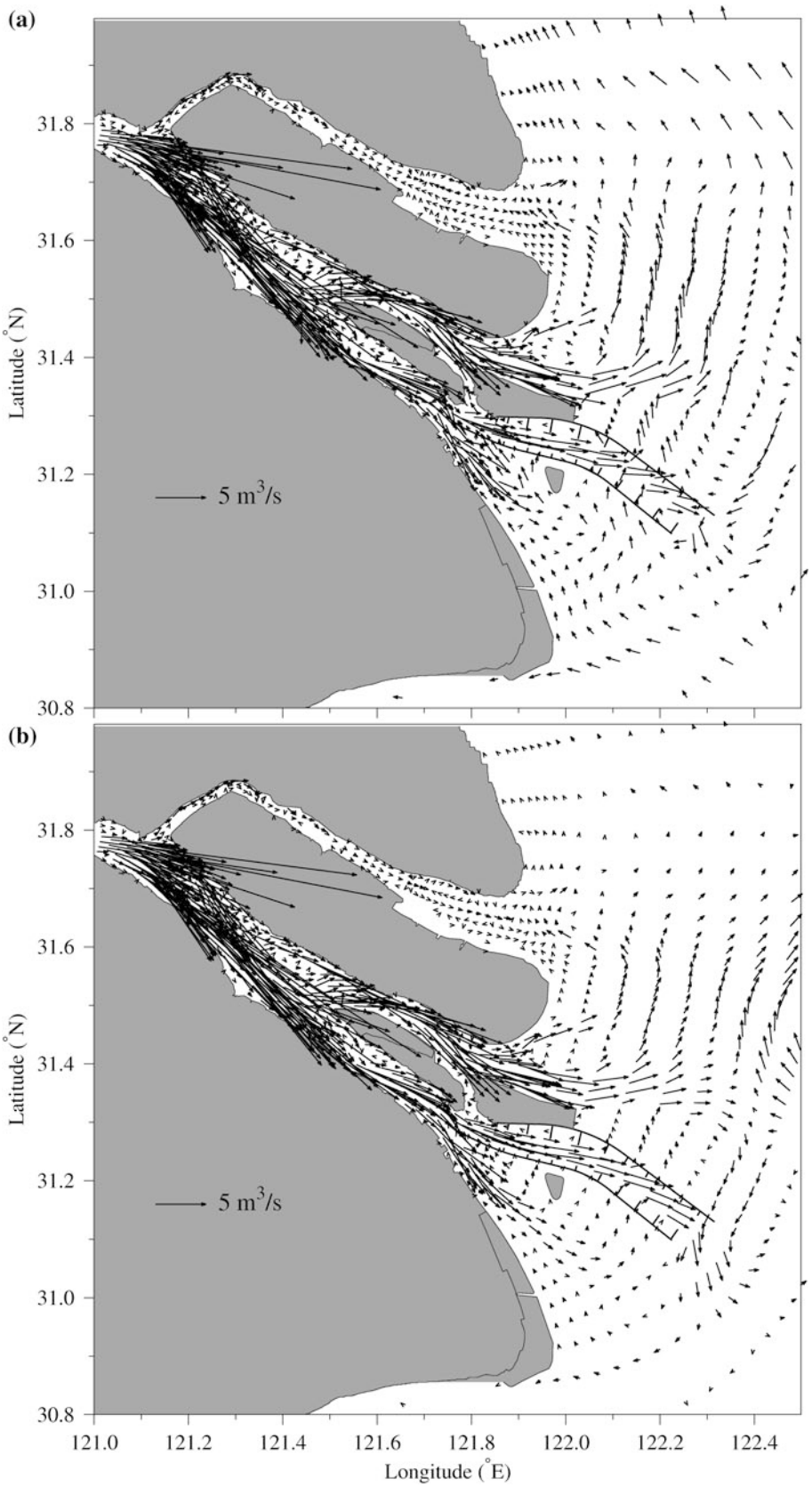

Fig. 2.7 Distribution of the NUWF during summer for: **a** spring tides; and **b** neap tides

Box 2.1 Saltwater Intrusion into the Changjiang Estuary

The combined effects of river discharge, tides, winds, mixing, and topography control saltwater intrusion into the Changjiang Estuary. The dominant feature of saltwater intrusion is the saltwater-spilling-over (SSO) from the NB into the SB (Fig. 2.1), which causes saltwater intrusion to have a complicated spatial and temporal variability in the SB. Saltwater intrusion mainly occurs in dry season. This is not only of significant scientific interest, but also has serious implications for the supply of fresh water to Shanghai. Before 2010, drinking water for Shanghai was mainly taken from the Huangpu River. However, with increasing population, the water quantity became insufficient and water quality was also not optimal. Now, the huge Qingcaosha Reservoir in the estuary supplies about 80 % of Shanghai's fresh water, but saltwater intrusion is a direct threat to the water supply in the dry season.

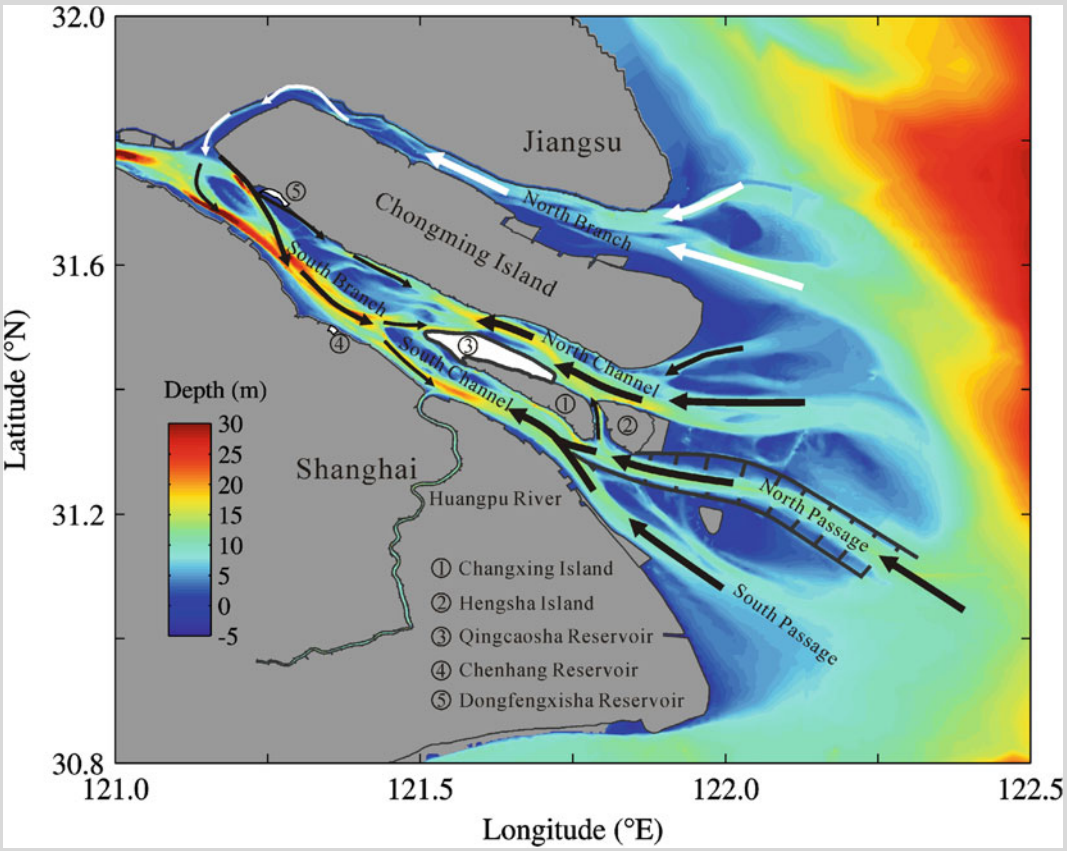

Map of the Changjiang Estuary, showing the pathways for saltwater intrusion (arrows) and the locations of reservoirs.

Although we have conducted intensive studies of saltwater intrusion into the Changjiang Estuary (Li et al. 2012), for brevity, we only outline the impacts of wind stress on saltwater intrusion in this section.

Previous studies have mainly focused on the effects of river discharge, tides, topography, and subtidal circulation (e.g., Shen et al. 2003). Some preliminary studies have used numerical experiments to examine the effect of wind stress on saltwater intrusion (e.g., Wu et al. 2010), but this cannot be thoroughly examined without long-term salinity data.

This subsection describes a detailed analysis of long-term salinity data from Chongxi station. A well-validated 3D numerical model was used to reproduce the salinity variability at Chongxi station during strong northerly winds, and to study the response of saltwater intrusion to different wind stresses based on a series of numerical experiments.

2.3.1 Impacts of Wind Stress on the SSO

A salinity gauging station was established at Chongxi (S2 in Fig. 2.8) in February 2009 to monitor the SSO, and an OBS-3A conductivity sensor was deployed for salinity

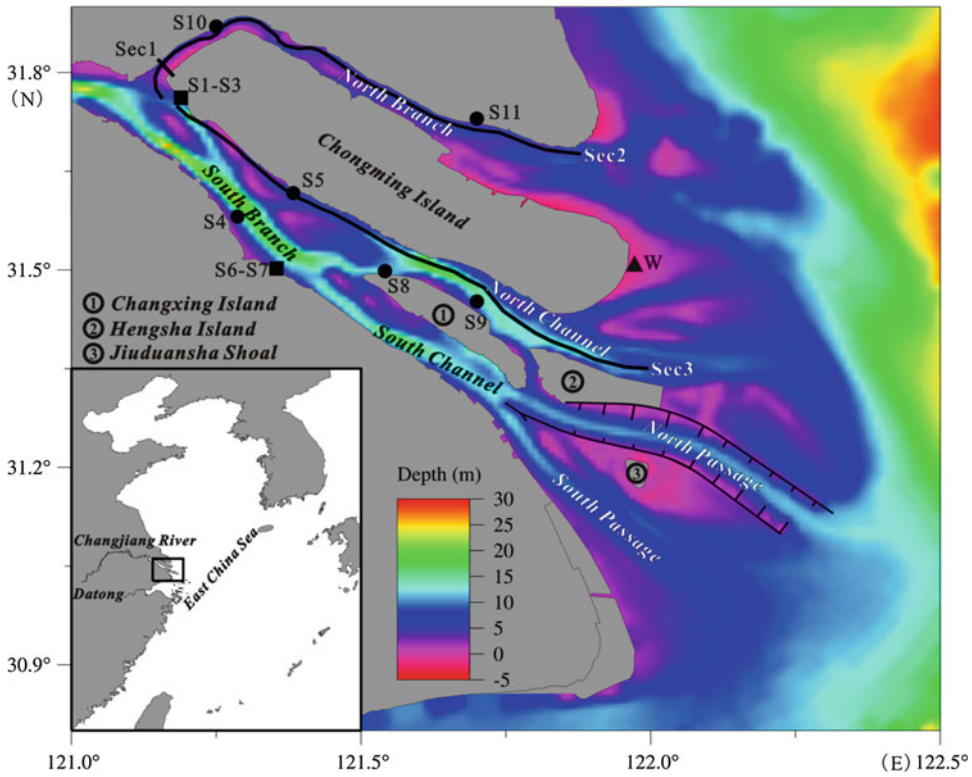

Fig. 2.8 Locations of observational stations and profiles. *S1* is Chongtou; *S2* is Chongxi; *S3* is Xinjian; *S4* is Taicang; *S5* is Nanmen; *S6* is Baogang; *S7* is Chenhang; *S8* is Qingcaosha A; *S9* is Qingcaosha B; *S10* is Qinglonggang; and *S11* is Qidong. The weather station in the eastern Chongming tidal flat is marked by a *black triangle*, and the three profiles (*Sec1*, *Sec2*, and *Sec3*) are indicated by *black lines*

measurements. The instrument was fixed at a depth of about 1 m below the water surface, and the sampling rate was 2 min.

The surface salinity was recorded between November 2009 and February 2010. During this period, the discharge of the Changjiang (Fig. 2.9a) was recorded at Datong station (Fig. 2.8); the water level (Fig. 2.9b) was recorded at Qinglonggang station (S10 in Fig. 2.8); and the wind speed and direction (Fig. 2.9c) were measured at the weather station in the eastern tidal flat of Chongming Island ("W" in Fig. 2.8). The surface salinity is shown in Fig. 2.9d.

Chongxi station is situated at the tip of the bifurcation of the SB and NB, where the salinity exhibits a semimonthly variation. In general, the salinity was higher during spring tides with a maximum value near 4 and was lower during neap tides with a minimum value below 0.5.

The results indicate that the tide plays an important role in determining the degree of saltwater intrusion at Chongxi station. Figure 2.9d shows that the SSO in December 2009 was weaker than in January 2010 during a spring tide, because the river discharge was higher in December 2009 than in January 2010. From November to early December in 2009, the river discharge was more than 13×10^3 m^3/s, which was greater than for the period from late December in 2009 to early January in 2010, when it was 12×10^3 m^3/s. This indicates that river discharge is another key control on the SSO, which is consistent with previous observations and studies (Shen et al. 2003; Wu et al. 2006).

It is also interesting that the salinity at Chongxi station increased to 2 during a neap tide on November 11–12, 2009. The river discharge of 14×10^3 m^3/s was constant over this period, but strong northerly winds occurred with a maximum wind speed of 12 m/s. A similar situation was repeated during February 11–12, 2010. At this time, the tide was moderate, but the salinity at Chongxi station increased anomalously to 3.7. This salinity value was higher than those measured either before or after spring tides. The river discharge was 14.5×10^3 m^3/s, but again, strong northerly winds prevailed with a maximum wind speed of 10 m/s. These results lead us to speculate that strong northerly winds tend to intensify the SSO.

2.3.2 Numerical Simulations

The 3D numerical model described in Sect. 2.2.2.1 was used to simulate the abnormal variations of salinity at Chongxi station during the neap tide on November 10–12, 2009, and during the moderate tide on February 11–12, 2010. The model was run from October 1, 2009, and January 1, 2010, respectively, with river discharge data from Datong station and wind speed from the weather station in the eastern tidal flats of Chongming Island.

The model successfully simulated the salinity variation during the neap tide at Chongxi station during November

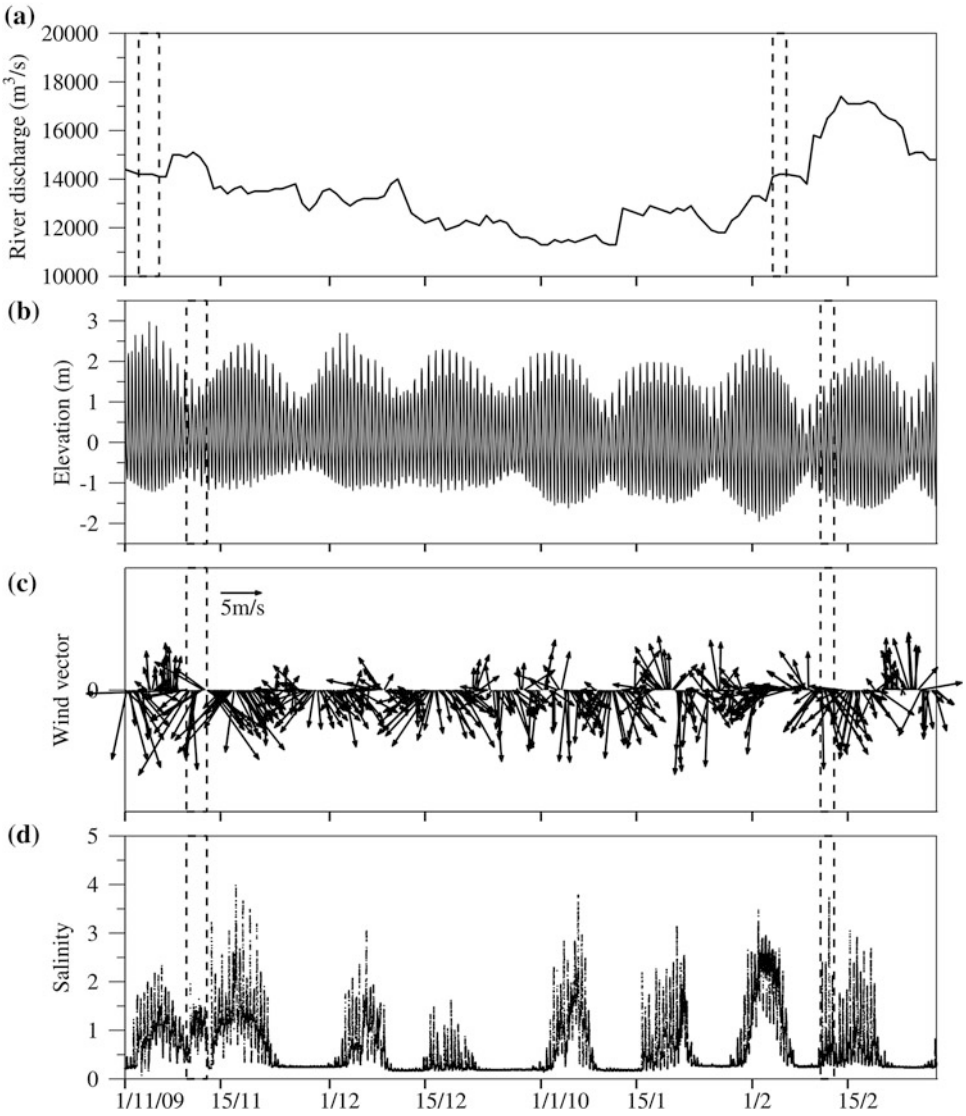

Fig. 2.9 In situ data measured from November 2009 to February 2010: **a** river discharge at Datong hydrographic station; **b** tidal level at Qinglonggang station; **c** wind vectors at the weather station in the eastern Chongming tidal flat; and **d** surface salinity at Chongxi station. The *dashed boxes* in panels **b**–**d** denote the periods of November 10–12, 2009, and February 11–12, 2010. *Dashed boxes* in panel **a** indicate the period seven days before that shown in panels **b**–**d**

10–12, 2009, as well as salinity during the spring tide of November 16–20, 2009 (Fig. 2.10d1). To examine the influences of wind stress on the SSO, the model was run again with half of the measured wind speed. The resulting salinity was correspondingly lower than for the measured data during the spring and neap tides (Fig. 2.10d2). For example, on November 10 and November 17, 2009, the simulated daily maximum salinity decreased from 2 and 3.5 to 1.5 and 3, respectively.

The model also reproduced the salinity variation at Chongxi station on February 11–12, 2010, during a moderate tide, and February 15–18, 2010, during a spring tide (Fig. 2.11d1). Simulated salinity that was generated by half the measured wind speed was lower than for in situ station data (Fig. 2.11d2). For example, on February 11–12, 2010, the simulated daily maximum salinity decreased from 3 and 3.5 to 2 and 2.5, respectively. These results demonstrate that strong northerly winds have a pronounced effect on enhancing the SSO.

2.3.3 Mechanisms of Wind Impact on Saltwater Intrusion

The results presented in the previous section show that an abnormal increase in salinity at Chongxi station during neap and moderate tides can be attributed to strong northerly winds. The mechanisms for the impact of wind speed/direction on saltwater intrusion as well as the SSO were investigated with a series of numerical experiments. The results

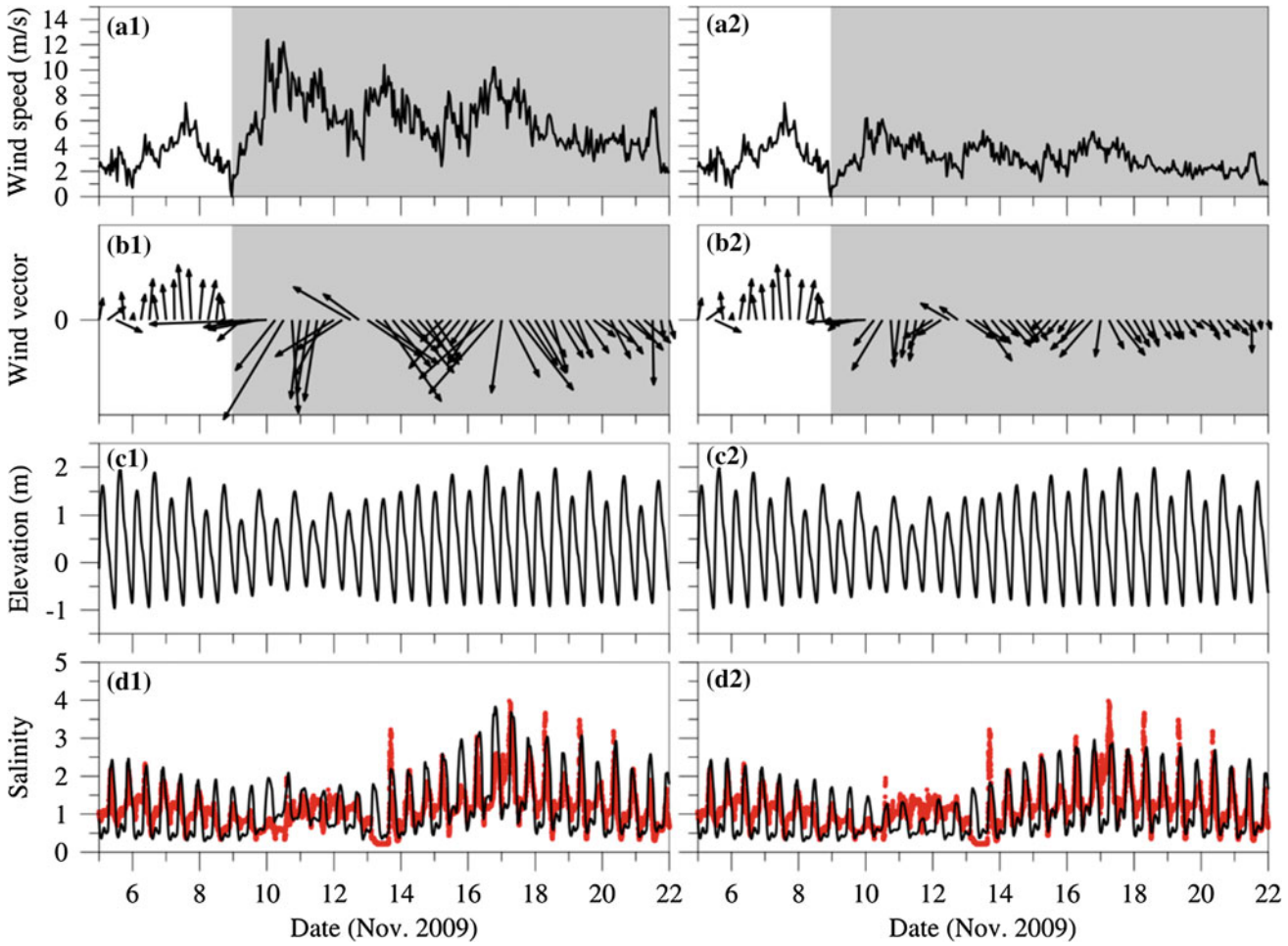

Fig. 2.10 Wind data, and simulated and measured surface salinity for November 5–22, 2009: **a1** measured wind speeds; **b1** wind vectors from the weather station in the eastern Chongming tidal flat; **c1** simulated tidal elevations; **d1** comparison of simulated surface salinity (*black solid line*) and measured data (*red dots*) at Chongxi station; **a2** half of the measured wind speeds; **b2** half of the measured wind vectors; **c2** simulated tidal elevations using half of the measured wind speeds and vectors; and **d2** comparison of simulated surface salinity (*black solid line*) and measured data (*red dots*) at Chongxi station using half the measured wind speeds and vectors

show that northerly and northwesterly winds have significant impacts on the enhancement of wind-driven circulation, causing saltwater intrusion into the NB and NC flows out of the SC, SP, and NP. For further details, see Li et al. (2012).

2.4 Dispersal of Riverine Plumes in the East China Sea

Dispersal of the plume off the Changjiang in summer is one of the most important physical processes in the East China Sea and Yellow Sea (e.g., Mao et al. 1963; Zhu and Shen 1997; Moon et al. 2010). Previous observations and studies have indicated the CDW riverine plume extends to the northeast in summer and flows south in a narrow band confined to the coast in winter (e.g., Mao et al. 1963; Beardsley et al. 1985; Zhu and Shen 1997).

The dispersal of the riverine plumes is strongly influenced by river discharge, the East Asia monsoon, tidal mixing, coastal currents, and continental-shelf circulation. The seasonal cycle of freshwater discharge from the Changjiang dominates the distribution of riverine plumes, especially in summer when peak river output occurs. Strong surface cooling and winds disrupt the vertical salinity stratification during winter, and it is re-stratified by strong heating during summer (Beardsley et al. 1985). Strong semidiurnal tidal currents over the bottom in the shallower regions can cause both strong tidal mixing and generate subtidal residual flow, which contributes to the plume distribution (Wu et al. 2011).

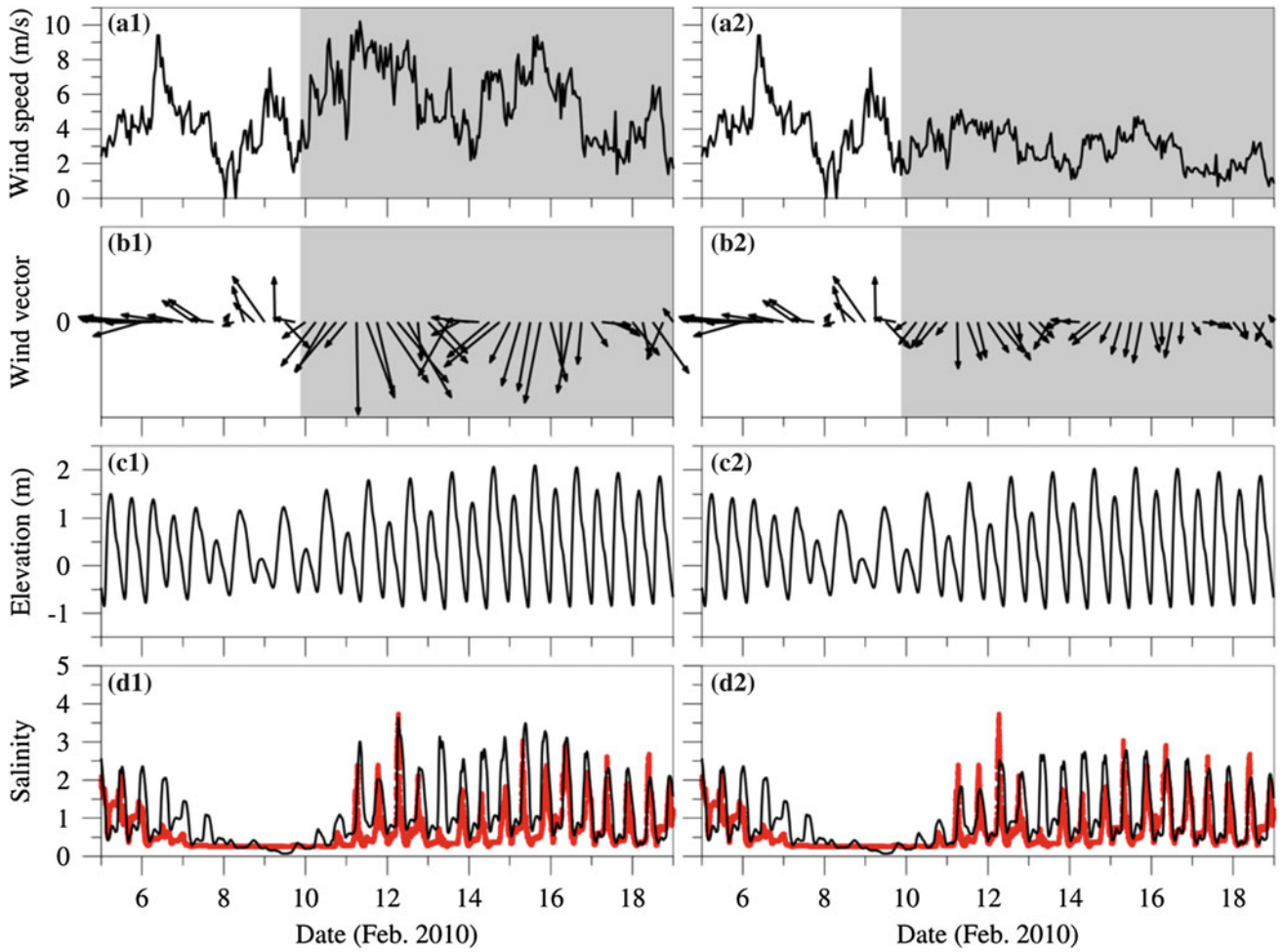

Fig. 2.11 Wind data, and simulated and measured surface salinity for February 5–19, 2010: **a1** measured wind speeds; **b1** wind vectors from the weather station in the eastern Chongming tidal flat; **c1** simulated tidal elevations; **d1** comparison of simulated surface salinity (*black solid line*) and measured data (*red dots*) at Chongxi station; **a2** half of the measured wind speeds; **b2** half of the measured wind vectors; **c2** simulated tidal elevations using half the measured wind speeds and vectors; and **d2** a comparison of simulated surface salinity (*black solid line*) and measured data (*red dots*) at Chongxi station using half the measured wind speeds and vectors

Mao et al. (1963) used salinity data to show, for the first time, that the CDW turns to the northeast in summer, but not to the south as would be expected from the Coriolis force. The southerly summer monsoon is the dominant factor in the northeastward extension of the plume (Zhu and Shen 1997; Chang and Isobe 2003). When the southerly wind speed exceeds 3 m/s, the extension of the plume is skewed to the northeast due to Ekman transport. The far-field diluted water joins the northeastward shelf-current system and flows out of the East China Sea and Yellow Sea region, through the Tsushima–Korea Strait where the year-round freshwater outflow is estimated to be at least 70 % of the total Changjiang river discharge (Isobe et al. 2002; Chang and Isobe 2003).

However, the plume pattern is highly variable in a large region near the Changjiang mouth, illustrating the very dynamic nature of CDW (Box 2.2). Although the plume eventually spreads to the northeast under the influence of the southerly monsoon in summer, the underlying mechanisms controlling its initial development and the variation near the river mouth are still poorly understood. Factors that are thought to be important are southerly winds (Zhu and Shen 1997); the high Changjiang runoff in summer (Le 1984); vortex stretching that results from increased depths offshore

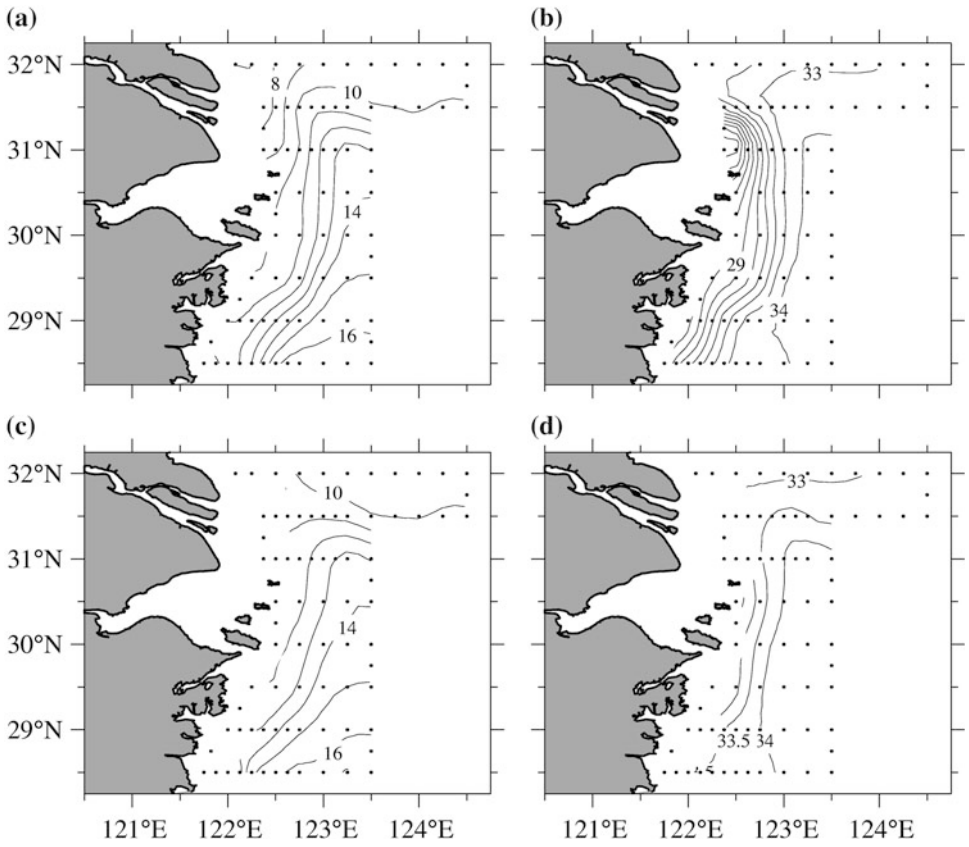

Fig. 2.12 Distribution of temperature and salinity from February 24 to March 10, 2001, for **a** temperature at 3 m depth; **b** salinity at 3 m depth; **c** temperature at 30 m depth; and **d** salinity at 30 m depth. The *dots* mark the observation sites

(Beardsley et al. 1985); basin-scale secondary cyclonic flow produced by the cold water dome in the Yellow Sea (Zhu et al. 1998); and the elevated sea surface that results from the TWC (Zhao 1991). Based on satellite images of surface suspended-sediment concentrations, Pu et al. (2002) reported that the distance and direction of the plume can change completely over a period ranging from less than one week to ten days.

Box 2.2 Extension of the Changjiang Riverine Plume

The Changjiang riverine plume extends to the northeast in summer and south along the coast in a narrow band in winter. The seasonal cycle of freshwater discharge from the Changjiang dominates the distribution of the riverine plume, especially in summer when peak river output occurs. The vertical salinity stratification is mixed in winter by strong surface cooling and wind-mixing and is re-stratified by strong heating during summer. The extension of the riverine plume is mainly controlled by river discharge, winds, and continental-shelf circulation. However, strong semidiurnal tidal currents in shallow regions can cause strong tidal mixing and generate subtidal residual flow, which also influences the plume distribution.

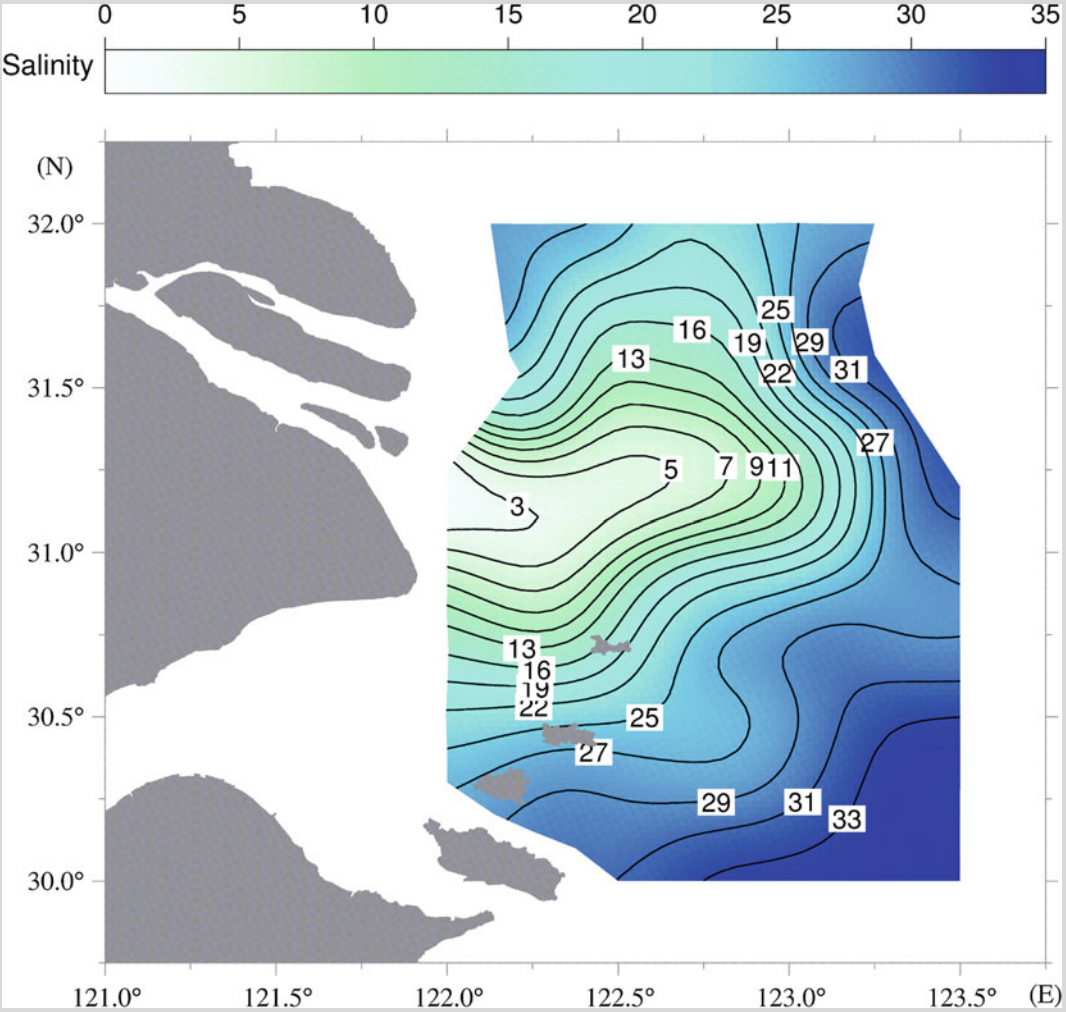

Extension of the Changjiang riverine plume in August 2008.

The dispersal of the plume is closely related to the circulation off the Changjiang Estuary, which includes the wind-driven current, Changjiang river discharge, the TWC, the East China Sea Coastal Current (ECSCC), and the Chinese Coastal Current (CCC) (Fig. 2.2). Due to the East Asia monsoon, which is southerly and stronger in winter, and northerly and weaker in summer, the southward Jiangsu Coast Current is stronger in winter and weaker in summer. Furthermore, under the influence of the monsoon, the Zhejiang Coast Current flows south in winter and north in summer (Beardsley et al. 1985).

A northwestward inflow of relatively warm and saline TWC water is found in the submerged valley located just offshore from the Changjiang mouth. This inflow is the source of the near-bottom saline water found in the lower part of the Changjiang Estuary. This near-bottom saline water is a permanent circulation feature in both winter and summer and has an important influence on dynamic processes in the estuary (Xiang et al. 2009).

For this study, ocean cruises were conducted off the Changjiang mouth almost every year since 2000. The Seabird CTD (Conductivity–Temperature–Depth) was used to measure salinity, temperature, and water depth. In this subsection, we use water temperature and salinity data to analyze the mechanisms that control the extension of the CDW. For brevity, we present winter observations from: (i) February 24 to March 10, 2001, in Sect. 2.4.1, and (ii) summer observations for June 16–30, 2003, in Sect. 2.4.2. Section 2.4.3 describes numerical simulations of the tidal modulation on the extension of the CDW.

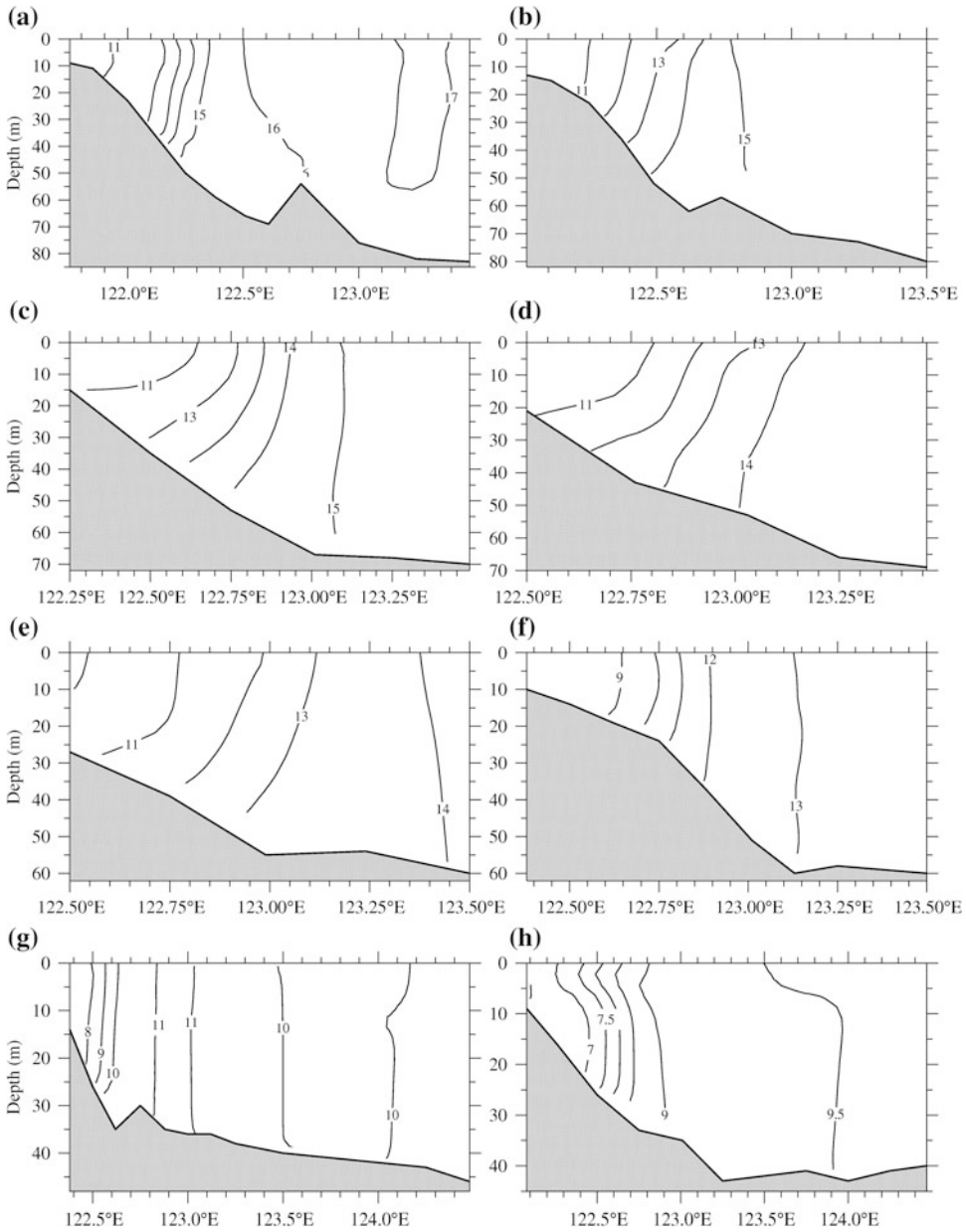

Fig. 2.13 Distribution of temperature along East–West transects for latitudes: **a** 28.5 °N; **b** 29.0 °N; **c** 29.5 °N; **d** 30.0 °N; **e** 30.5 °N; **f** 31.0 °N; **g** 31.5 °N; and **h** 32.0 °N

2.4.1 Extension of the CDW in Winter

The survey was conducted from February 24 to March 10, 2001, in the area bounded by 28.5–32.0 °N and 124.5 °E (Fig. 2.12). There were 79 grid stations and 8 East–West transects, with a high station resolution in the salinity front area just off the river mouth.

Figure 2.12 shows the horizontal distributions of temperature and salinity in winter at depths of 3 and 30 m. The CDW extended south from the river mouth in a narrow band along the coast. As the Changjiang water is fresher and colder than seawater in winter, the water farther from the coast was more saline with higher temperatures. A tongue of this water, brought by the northward-flowing TWC, extended to the northeast and entered the submerged valley off the Changjiang. Mixing between the CDW and the TWC water formed a narrow and strong temperature and salinity front along the coast.

The vertical profiles of temperature and salinity (Figs. 2.13 and 2.14) along the East–West transects show that they were well mixed and lower near the coast. Along the transect at 28.5 °N, the temperature and salinity ranged from 11 to 17 °C and from 28 to 34, respectively. The vertical temperature profile was relatively uniform, but the salinity profile had more vertical structure. Along the transect at 29.0 °N, temperature and salinity were also well mixed and ranged from 11 to 15 and from 27 to 34, respectively.

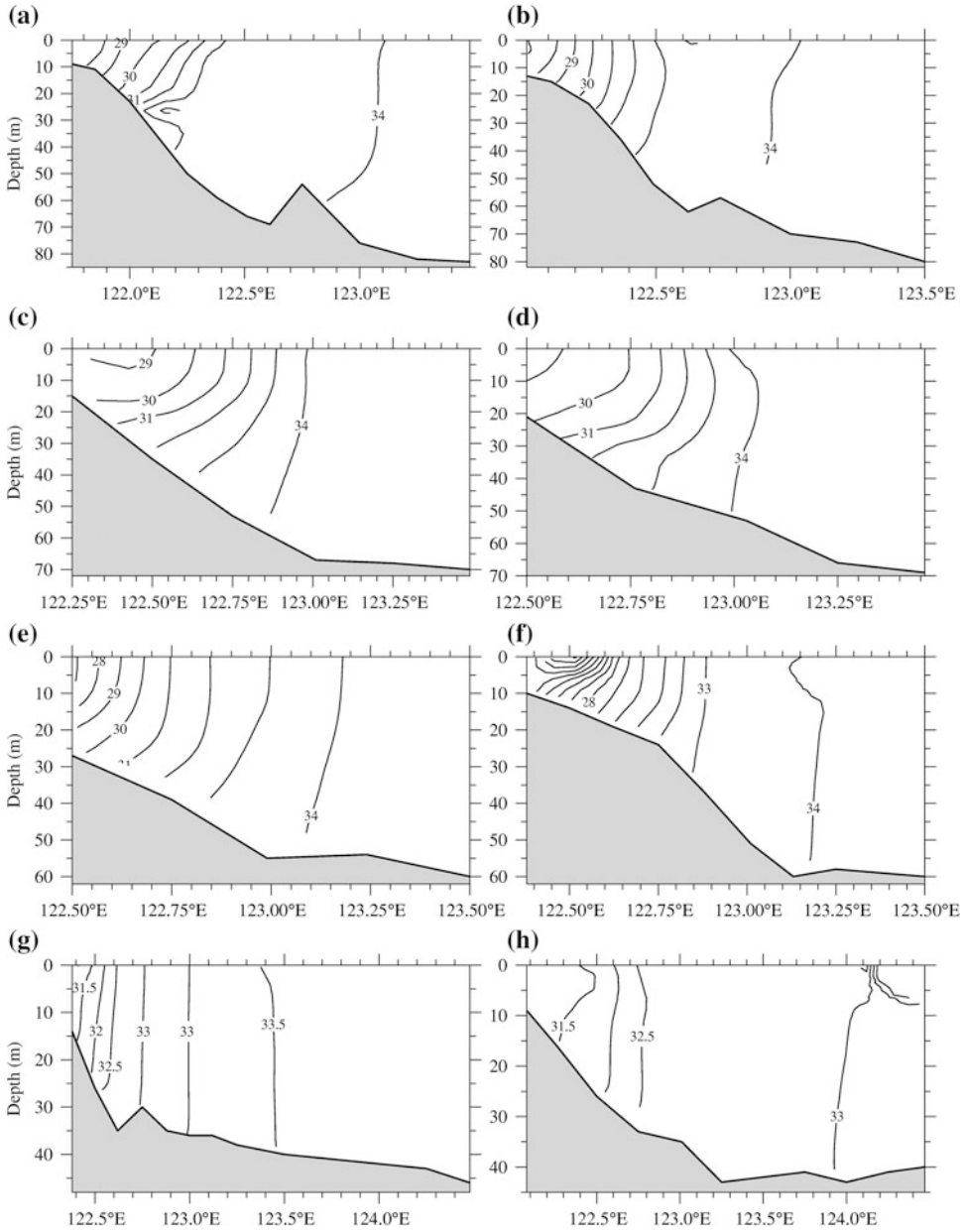

Fig. 2.14 Distribution of salinity along east–west transects for latitudes: **a** 28.5 °N; **b** 29.0 °N; **c** 29.5 °N; **d** 30.0 °N; **e** 30.5 °N; **f** 31.0 °N; **g** 31.5 °N; and **h** 32.0 °N

Along the transects at 29.5, 30.0, and 30.5 °N, the temperature and salinity contours show a seaward bend along the slope bottom, indicating downwelling along the coast. The dynamic mechanism for the downwelling was that strong northerly winds drove the surface water onshore by Ekman transport and, to conserve mass, produced an offshore current along the slope bottom.

Along the transect at 31.0 °N, there was a small domain plume near the river mouth where the Changjiang water empties into the sea. Along the transect at 31.5 °N, there was a strong temperature and salinity front along the coast, which was vertically uniform. Along the northern transect at 32.0 °N, the temperature was lower than along the southern transects.

2.4.2 Extension of the CDW in Summer

A survey off the Changjiang mouth was conducted during June 16–30, 2003, in the region bounded by 29.5–32.5 °N and 124.5 °E. The cruise completed a total of 6 East–West transects and collected data at 80 different locations (Fig. 2.15). Higher resolution observations were taken in the thermal front and in areas with frequent high red tides or algae blooms.

The salinity at a depth of 1.5 m below the surface (Fig. 2.16) shows that the CDW formed a bimodal shape as it extended away from the river mouth, with one limb moving to the southeast, and another larger limb moving to the northeast.

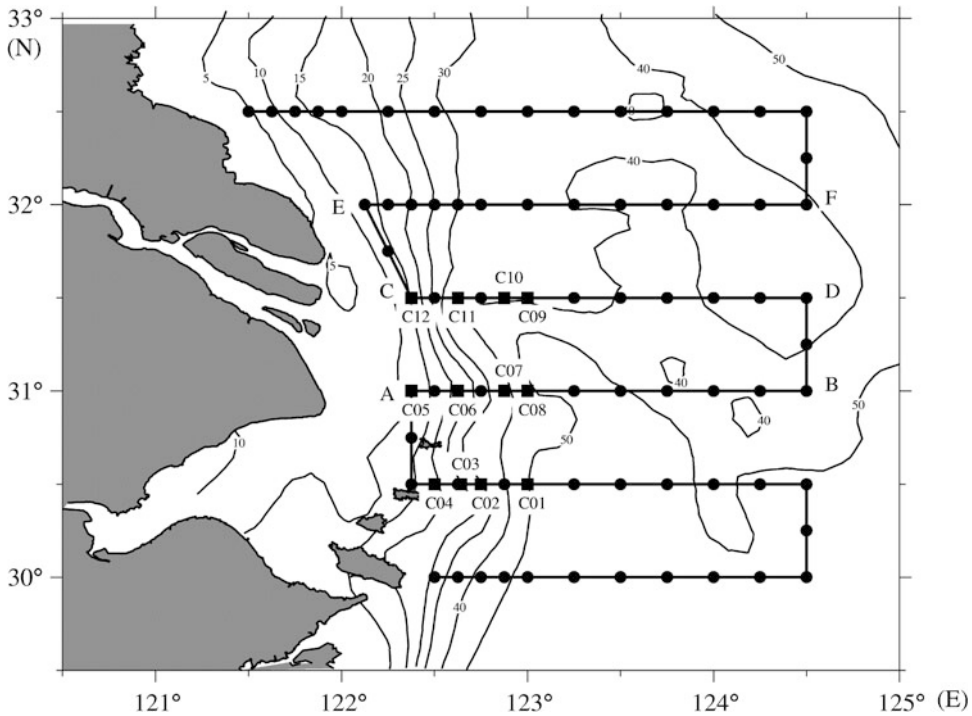

Fig. 2.15 Cruise observations off the Changjiang mouth during June 16–30, 2003. The *thick solid line* is the cruise route, and *thin lines* are the isobaths (in meters). The *blank circles* show the positions of the measurement stations, and *black squares* are the water-sample stations. The labels "AB," "CD," and "EF" mark transects located at latitudes 31, 31.5, and 32 °N, respectively

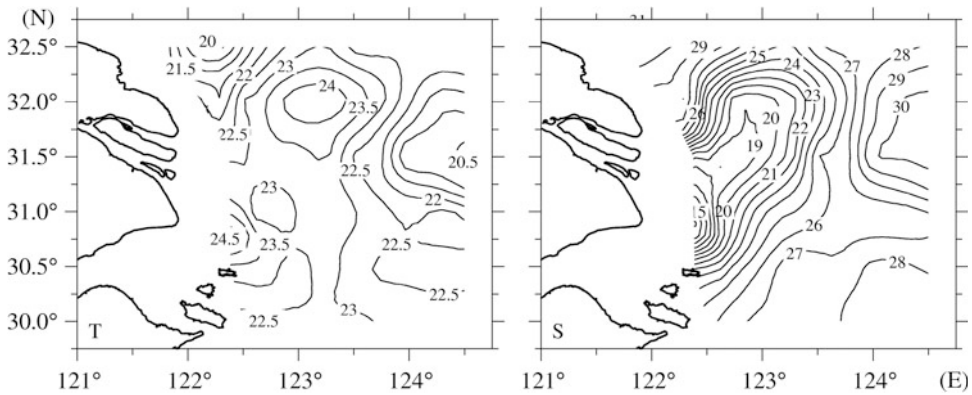

Fig. 2.16 Horizontal distribution of temperature (*left*) and salinity (*right*) at a depth of 1.5 m below the surface. The unit for temperature (*T*) is °C, and the unit for salinity (*S*) is psu

The Changjiang river discharge at Datong hydrographic station during the observational period was between 32×10^3 and 40×10^3 m^3/s. This was lower than the mean value of 43×10^3 m^3/s in mid- and late June 2003. This suggests that lower river discharges promote the northeast extension of the CDW.

The temperature of the Changjiang estuary water was higher than the seawater in summer. After entering the sea, this plume of high-temperature water had the same bimodal shape, but an area of colder water with temperatures of between 22.5 and 23 °C appeared on the west side of the submerged valley. Previous observations and analysis indicated that this was produced by the bottom Ekman-layer effect on the north-flowing TWC, and a baroclinic effect induced by freshwater–saltwater mixing (Zhu 2003).

In view of the distribution of temperature and salinity along transects AB, CD, and EF in Figs. 2.15, 2.16, and 2.17, the plume produced by the CDW was very significant and located above a depth of approximately 10 m. The CDW gradually extended eastward from the southern transact, AB, to the northern transect, EF. The high-temperature water in the plume indicates that the Changjiang Estuary waters flowing into the East China Sea had relatively high temperatures and low salinities, with an obvious thermocline and halocline.

The temperature and salinity contours bend downward at 123.5 °E along the section AB, implying downwelling,

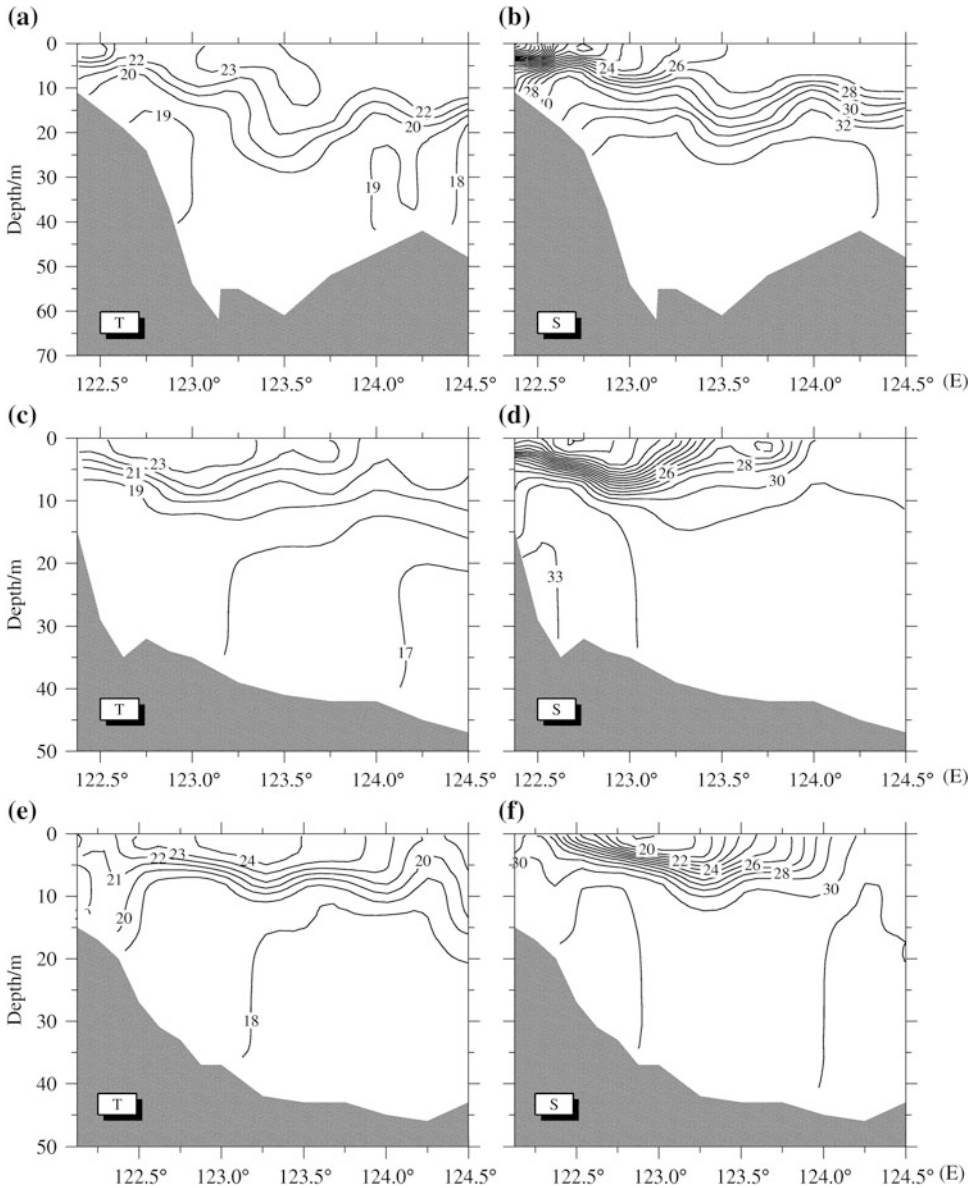

Fig. 2.17 Vertical distribution of temperature (*left panel*) and salinity (*right panel*) along transects AB, CD, and EF (shown in Fig. 2.15)

while they bend upward on the west side, indicating upwelling with a clockwise circulation. The bottom of the thermocline was at approximately 15 m depth, with the exception of the downwelling region where it deepened to 30 m. The seawater in the submerged valley had low temperatures and high salinities, and the upward-bending contours in the west of the valley indicated that upwelling also occurred in this area (Zhu 2003).

2.4.3 Numerical Simulation of Tidal Modulation on the Extension of the CDW

The tidal modulation of the CDW is introduced briefly in this subsection, and further details can be found in Wu et al. (2011). Simulations of the tidal modulation of the CDW were made using a numerical model that encompasses the entire East China Sea and Yellow Sea, with higher resolution grids around the river mouth. Skill assessments, based on the model simulations forced by real observations, indicated that the model can reproduce the tides, shelf currents, and temporal–spatial variations of the CDW. Comparisons of the model-validation simulation, both with and without the tidal forcing, further confirmed the critical role played by tides in modulating the CDW (Wu et al. 2011).

Two experiments were initially conducted in which the wind forcing and the shelf currents were excluded. Without the tidal forcing, we found that the CDW extends strongly to the north along the Jiangsu Coast, a phenomenon that has rarely been observed, but frequently occurs in model studies

that do not include tidal forcing. When the tide is superimposed, however, the northward extension of the CDW along the coast disappears. The strong tide along the Jiangsu Coast is sufficient to mix the water column, resulting in the formation of a strong along-coast salinity gradient to the north of the Changjiang mouth, which obstructs the northward extension of the plume (Wu et al. 2011).

The model results also showed that spring–neap tidal variations result in a distinguishable spatial pattern. During the spring tide, there is a near-field plume located inside the 30-m isobath. At its frontal edge, the subtidal momentum is balanced by momentum advection and the Coriolis force via a mechanism of tidal rectification, which drives a residual current mainly to the southeast. Around the head of the submarine valley, an anticyclonic rotating plume-bulge occurs, as a result of the local high-subtidal sea level that can result from tidal asymmetry. The bulge rotates the CDW to the northeast at about 122.5 °E (Wu et al. 2011).

Considering that the wind and the shelf currents were not included in this experiment, this indicates that the northeastward extension is an intrinsic property of the CDW. In addition, the near-field plume and the bulge illustrate a bi-directional plume structure separated from the head of the submarine valley. During the neap tide, because of the reduced tidal energy, the effects of tidal rectification and tidal asymmetry become small, and the near-field plume therefore extends farther east and the bulge is less evident.

Further experiments, conducted by adding 4 m/s southerly winds and shelf currents to the model, indicated that although the wind forcing ultimately drives the CDW to the northeast in the far field, the dynamics of the tidal modulation are robust near the river mouth. The near-field plume is almost identical to the plume formed without wind forcing. Although the bulge merges into the far-field plume due to the intensified mixing, the CDW rotates to the northeast in almost the same location as the plume formed without wind forcing. Furthermore, the bi-directional plume structure is maintained and is even more pronounced. If the tidal forcing is excluded, however, the southeast branch of the CDW disappears.

It was also found that, during the spring tide, the bottom saline water can penetrate the river plume by convective transport along the slope, thereby cutting off the CDW and forming a detached zone of freshwater. In summary, these results show that the tide has an important influence on the extension of the CDW in the near field, while the wind has a dominant effect in the far field (Wu et al. 2011).

2.5 Summary

The temporal–spatial variations of tides, as well as the tide's harmonic constituents, form, and distortion in the Changjiang Estuary were analyzed based on in situ hourly data from tidal gauging stations. Significant semidiurnal, fortnightly, and seasonal tidal variations were found. Mean monthly water levels varied seasonally in concert with river discharge, which reached its peak during the flood season, and dropped to its lowest values during the dry season. The maximum monthly tidal range exhibited two peaks, in March and September, and fell to its lowest values in June and December each year.

As the tidal wave propagates up-estuary, the tidal range in the SB becomes smaller than that in the lower reaches due to friction and reduced river discharge. In the NB, the tidal forcing is amplified due to the funnel-shaped topography and the weaker influence of river discharge.

Harmonic analysis showed that tides around the Changjiang Estuary are dominated by four semidiurnal constituents (M_2, S_2, N_2, and K_2); four diurnal constituents (K_1, O_1, P_1, and Q_1); and three shallow-water constituents (M_4, MS_4, and M_6). The tidal form, distortion, and asymmetry numbers were calculated using harmonic constants, so that the key tidal features could be characterized.

Numerical simulations of the circulation (i.e., residual current) in the Changjiang Estuary show that flow in the SB has a speed of approximately 0.1 m/s and 0.5 m/s when the river discharge is 11×10^3 and 50×10^3 m^3/s, respectively. Only a small amount of river water flows into the NB due to its shallow topography.

The salinity measured at Chongxi gauging station during a neap tide and moderate tide rose anomalously when northerly winds were strong. This demonstrated that wind stress enhances the SSO. To further investigate this phenomenon, a 3D numerical model was used to reproduce the anomalous salinity at Chongxi station. The results showed that when the wind speed was reduced by half, the salinity was significantly reduced. Additional numerical experiments, using different wind speeds and directions, also indicated that the wind has an important effect on saltwater intrusion.

Data collected off the Changjiang mouth in winter show that the CDW extended south in a narrow band along the coast. A tongue of relatively high-temperature and high-salinity water, brought by the northward-flowing TWC, flows into the submerged valley and can reach the area just off the Changjiang mouth. Mixing between the relatively low-temperate and low-salinity CDW water and the TWC water formed a strong temperature and salinity front along the coast. A small domain plume front was also observed near the river mouth, and downwelling occurred along the coast due to strong onshore winds, which produced Ekman transport in the surface waters and an offshore current along the middle and bottom layers.

A survey off the Changjiang mouth showed that the CDW extended offshore with a significant thermocline and halocline. It had a bimodal structure in summer, with one main

Table 2.5 Mean monthly river discharge (RD, m^3/s) and water volume (WV, 10^8 m^3) of the Changjiang from 1950 to 2010 at Datong hydrographic station

Month	1	2	3	4	5	6	7	8	9	10	11	12
RD	11184	12058	16300	24061	33488	40454	49848	44149	39909	32332	22552	14063
WV	299.6	291.7	436.6	623.7	896.9	1048.6	1335.1	1182.5	1034.4	866.0	584.5	376.7

branch extending to the northeast and another more minor branch extending to the southeast. There was upwelling along the west slope of the submerged valley due to the baroclinic effect and the bottom Ekman effect of the northward-flowing TWC. Numerical simulations indicated that the tide has an important effect on the dispersal of the riverine plume through tidal mixing.

The extension of the CDW is controlled mainly by the river discharge, winds, and tides; however, as observations of the CDW generally take one survey vessel between five to eight days, the wind and tide change during the observation period. For this reason, more than one vessel is needed to synchronize the data. For numerical simulations of the dispersal of the riverine plume, the combined effects of river discharge, wind, tide, and continental-shelf current are important, and each dynamic factor should be correctly parameterized. The numerical simulation showed that the tide has an important influence on the extension of the CDW in the near field, whereas the wind has a distinct effect in the far field (Table 2.5).

Acknowledgments This work was based on research started in the early 1990s, with financial support from the Natural Science Foundation of China (Grant numbers: 40376027, 40776012, 40976056, 40721004, 41176071, and 41021064); the Major Program of Shanghai Science and Technology Committee (Grant numbers: 05XD14006 and 08231200102); and the Ministry of Science and Technology of China (Grant numbers: G1999043803, 2010CB951201, and 2011CB409801). We thank colleagues and students from the State Key Laboratory of Estuarine and Coastal Research (ECNU) for support in collecting field observations, numerical simulations, and laboratory analyses.

References

Beardsley R, Limburner R, Yu H, Cannon GA (1985) Discharge of the Changjiang (Yangtze River) into the East China Sea. Cont Shelf Res 4:57–76

Blumberg AF (1994) A primer for ECOM-si. Technical report of HydroQual, Mahwah

Blumberg AF, Mellor GL (1987) A description of a three-dimensional coastal ocean circulation model. In: Heaps NS (ed) Three-dimensional coastal ocean models. American Geophysical Union, Washington D.C, pp 1–16

Chang PH, Isobe A (2003) A numerical study on the Changjiang diluted water in the yellow and East China Seas. J Geophys Res 108 (C9):3299. doi:10.1029/2002JC001749

Chen ZY (1980) Tidology. Science Press, Beijing, p 301

Chen C, Zhu JR, Ralph E, Green SA, Budd JW, Zhang FY (2001) Prognostic modeling studies of the Keweenaw current in lake superior, part I: formation and evolution. J Phys Oceanogr 31:379–395

Choi BH (1980) A tidal model of the Yellow Sea and Eastern China Sea. Korea Ocean Research and Development Institute (KORDI) report, 72 pp

Editorial Board For Marine Atlas (1992) Ocean atlas in Huanghai Sea and East China Sea (hydrology). China Ocean Press, Beijing

Galperin B, Kantha LH, Hassid S, Rosati A (1988) A quasi-equilibrium turbulent energy model for geophysical flows. J Atmos Sci 45:55–62

Geyer WR (1993) The importance of suppression of turbulence by stratification on the estuarine turbidity maximum. Estuaries 16:113–125

Ianniello JP (1977) Tidally induced residual currents in estuaries of constant breadth and depth. J Mar Res 4:754–786

Isobe A, Ando M, Watanabe T, Senjyu T, Sugihara S, Manda A (2002) Freshwater and temperature transport through the Tsushima-Korea Straits. J Geophys Res 107(C7):3065. doi:10.1029/2000JC00702

Large WS, Pond S (1981) Open ocean momentum flux measurements in moderate to strong winds. J Phys Oceanogr 11:324–406

Le K (1984) A preliminary study of the path of the Changjiang diluted water. Oceanologia Et Limnologia Sinca 15(2):157–167 (in Chinese)

Li L, Zhu JR, Wu H, Wang B (2010) A numerical study on the water diversion ratio of the Changjiang Estuary in the dry season. Chin J Oceanol Limnol 28(3):700–712

Li L, Zhu JR, Wu H (2012) Impacts of wind stress on saltwater intrusion in the Yangtze Estuary. Sci China Earth Sci 55(7):1178–1192. doi:10.1007/s11430-011-4311-1

Lü X, Qiao F, Xia C, Zhu J, Yuan Y (2006) Upwelling off the Yangtze river estuary in summer. J Geophys Res 111:C11S08. doi:10.1029/2005JC003250

Mao H, Gan Z, Lan S (1963) Preliminary study on the Changjiang diluted water and its mixing natures. Oceanologia Et Limnologia Sinca 5(3):183–206 (in Chinese)

Mellor GL, Yamada T (1974) A hierarchy of turbulence closure models for planetary boundary layers. J Atmos Sci 33:1791–1896

Mellor GL, Yamada T (1982) Development of a turbulence closure model for geophysical fluid problem. Rev Geophys 20:851–875

Moon JH, Hirose N, Yoon JH, Pang IC (2010) Offshore detachment process of the low-salinity water around Changjiang bank in the East Chinese Sea. J Phys Oceanogr 40:1035–1053

Pritchard DW (1956) The dynamic structure of a coastal plain estuary. J Mar Res 15:33–42

Pu Y, Huang W, Xu J (2002) The spreading direction change of the Changjiang River diluted water in 7–10 days. J East China Sea 20:1–5 (in Chinese)

Qiu C, Zhu JR (2013) Influence of seasonal runoff regulation by the three gorges reservoir on saltwater intrusion in the Changjiang River Estuary. Cont Shelf Res 71:16–26

Shen HT, Mao ZC, Zhu JR (2003) Saltwater intrusion in the Changjiang Estuary. China Ocean Press, Beijing (in Chinese)

Simpson JH, Brown J, Matthews J, Allen G (1990) Tidal straining, density current, and stirring in the control of estuarine stratification. Estuaries 13:125–132

Smagorinsky J (1963) General circulation experiments with the primitive equations., I. The basic experiments. Mon Weather Rev 91:99–164

Su J, Yuan Y (2005) Oceanography of China Seas. China Ocean Press, Beijing, p 367

Wu H, Zhu JR (2010) Advection scheme with 3rd high-order spatial interpolation at the middle temporal level and its application to saltwater intrusion in the Changjiang Estuary. Ocean Model 33:33–514

Wu H, Zhu JR, Chen BR, Chen YZ (2006) Quantitative relationship of runoff and tide to saltwater spilling over from the North Branch in the Changjiang Estuary: A numerical study. Est Coast Shelf Sci 69:25–132

Wu H, Zhu JR, Choi BH (2010) Links between saltwater intrusion and subtidal circulation in the Changjiang Estuary: A model-guided study. Cont Shelf Res 30:1891–1905

Wu H, Zhu JR, Shen J, Wang H (2011) Tidal modulation on the Changjiang River plume in summer. J Geophys Res 116:C08017. doi:10.1029/2011JC007209

Xiang YY, Zhu JR, Wu H (2009) The impact of the shelf circulations on the saltwater intrusion in the Changjiang Estuary in winter. Prog Nat Sci 19(2):192–202 (in Chinese)

Zhao B (1991) On the extension of Changjiang diluted water. Acta Oceanol Sin 13(5):600–610 (in Chinese)

Zhu JR, Shen HT (1997) Extension mechanisms of Changjiang diluted water. East China Normal University Press, Shanghai (in Chinese)

Zhu JR, Xiao CY, Shen HT (1998) Numerical model simulation of expansion of Changjiang diluted water in summer. Acta Oceanol Sin 20:13–22 (in Chinese)

Zhu JR (2003) Dynamic mechanism of the upwelling on the west side of the submerged river valley off the Changjiang mouth in summertime. Chin Sci Bull 48(24):2754–2758

Zhu JR, Wu H, Li L, Wang B (2010) Saltwater intrusion in the Changjiang Estuary in the extremely drought hydrological year 2006. J East China Normal Univ (Nat Sci) 4:1–6, 25 (in Chinese)

http://www.springer.com/978-3-319-16338-3

Ecological Continuum from the Changjiang (Yangtze River) Watersheds to the East China Sea Continental Margin

Zhang, J. (Ed.)

2015, XIV, 201 p. 140 illus., 87 illus. in color., Hardcover
ISBN: 978-3-319-16338-3